An original model of brain infection identifies *B Streptococcus* lipoprotein Blr as a ligand exploiting host endocytosis for blood-brain barrier crossing.

Billel Benmimoun[1], Florentia Papastefanaki[2], Bruno Périchon[3], Katerina Segklia[2], Nicolas Roby[1], Vivi Miriagou[4], Shaynoor Dramsi[3], Rebecca Matsas[2] and Pauline Spéder[1,*]

1. Institut Pasteur, Brain plasticity in response to the environment, CNRS, UMR3738, Paris, France.
2. Cellular and Molecular Neurobiology, Stem Cells Lab, Department of Neurobiology, Hellenic Pasteur Institute, Athens, Greece.
3. Institut Pasteur, Unité de Biologie des Bactéries Pathogènes à Gram-positif, CNRS UMR 2001, Paris, France
4. Laboratory of Bacteriology, Department of Microbiology, Hellenic Pasteur Institute, Athens, Greece.

<u>*Corresponding author:</u>

Pauline Spéder, PhD
Department of Developmental and Stem Cell Biology
Institut Pasteur/CNRS UMR3738
Bâtiment Jacques Monod, 1er étage
25 rue du Docteur Roux
PARIS 75015
E-mail : pauline.speder@pasteur.fr
Phone: + 33 1 45 68 89 78

Abstract

Pathogens able to cross the blood-brain barrier (BBB) induce long-term neurological sequelae and death. Understanding how neurotropic pathogens bypass this barrier is a prerequisite to devise therapeutic strategies. Here we propose an innovative model of brain infection in the developing Drosophila brain, combining whole brain explants with *in vivo* systemic infection. Several mammalian pathogens were able to cross the Drosophila BBB, including *Group B Streptococcus* (GBS). Amongst GBS surface components, lipoproteins, and in particular Blr, were important for BBB crossing and virulence in Drosophila. Further, we identified LDL receptor LpR2, expressed in the BBB, as a putative receptor for Blr, allowing GBS translocation through endocytosis. Finally, we demonstrated that Blr is required for BBB crossing in a murine model of infection. Our results support the relevance of Drosophila for studying host-pathogen interactions and identify a new mechanism by which pathogens exploit host barriers to generate brain infection.

Introduction

Central nervous system (CNS) infections are rare although extremely damaging. They lead to fatal outcomes and long-term neurological disabilities in surviving infants and adults, including cognitive deficit and motor impairment (John et al., 2015). CNS infections are caused by the entry of pathogenic agents – bacteria, fungi or viruses, from the systemic environment into the CNS, provoking neuroinflammation and cellular damages.

A major route for CNS infection is the bloodstream, which pathogens enter after crossing the epithelial barriers of the skin and the gut (Cain et al., 2019; Dando et al., 2014; Doran et al., 2013), and in which they circulate as free particles or carried by blood cells (Kristensson, 2011). To infect the brain, pathogens must ultimately bypass an additional guardian: the blood-brain barrier (BBB) (Coureuil et al., 2017). The BBB is both a selective physical and chemical filter, enabling neuroprotective functions (Daneman and Prat, 2015). In higher vertebrates, brain microvascular endothelial cells form the core structure of the BBB. These cells are equipped to provide selective insulation, harboring intercellular tight junctions, absence of fenestrae, and asymmetrically localised transport systems (Saunders et al., 2016; Siegenthaler et al., 2013). These unique features distinguish brain microvascular endothelial cells from peripheral endothelial cells, and allow them to control ion, nutrient, and hormone transport ensuring ionic homeostasis and neuronal functions (Lampron et al., 2013; Weiler et al., 2017). The BBB also includes perivascular pericytes, glial astrocytes and a basal membrane made of extracellular matrix, which regulate BBB integrity and endothelial functions (Obermeier et al., 2013; Siegenthaler et al., 2013). This complex set of interlinked layers behaves as a double-edge sword for the organism: it restricts the entry of pathogens as well as therapeutic molecules, such as antibiotics (Banks, 2012; Daneman, 2012).

Pathogens that manage to cross the BBB thus secure their access to the CNS, where they tend to be immunologically-protected. Accordingly, neuro-invasive, neurotropic pathogens have developed intricate mechanisms that allow them to cross this layer and invade the CNS (Cain et al., 2019; Coureuil et al., 2017; Dando et al., 2014). Three main strategies have been proposed so far: transcellular, paracellular and Trojan horse. The transcellular entry occurs through a receptor-mediated mechanism or pinocytosis, while the paracellular mechanism follows the increase of BBB permeability due to tight junction disruption. The Trojan horse mechanism uses infected blood cells which transmigrate from the periphery to the CNS. It has been proposed that pathogens could actually use several of these routes to invade the brain (Coureuil et al., 2017).

So far, most of this knowledge comes from *in vitro* models of BBB (Jackson et al., 2019; Sivandzade and Cucullo, 2018) where a monolayer of endothelial cells are co-cultured with pericytes and astrocytes in transwells (Bergmann et al., 2018). However, these models still display a lot of variations in their tightness depending on the endothelial cells used and thus reproducibility is still a major issue. Despite induced pluripotent stem cell-related advances (Bergmann et al., 2018) and new set ups like microfluidic organ-on-chips (Heidari and Taylor, 2018), these models struggle to recapitulate complex parameters crucial to BBB properties, including 3D architecture and dynamic cellular interactions. Animal models, mostly mice and rats, but also zebrafish, exist and have provided essential contributions to mechanistic explorations (Dando et al., 2014; Jackson et al., 2019), including revisiting results from *in vitro* models (Disson and Lecuit, 2013). Manipulating these organisms to reach cellular resolution and causal relationships is nevertheless still highly challenging. Cost and ethical issues also hinder their extensive use.

Drosophila is a powerful and tractable model system, with unrivalled genetics. It has been very successful in identifying conserved molecular mechanisms in innate immunity, such as the Toll pathway (Bier and Guichard, 2012; Lemaitre and Hoffmann, 2007; Péan and Dionne, 2014). Most studies focused on systemic and epithelial immunity (skin and gut) (Bergman et al., 2017; Ferrandon, 2013), albeit one elegant study assessed the CNS inflammation mechanism during Zika virus infection in adults (Liu et al., 2018). Strikingly, many aspects of mammalian neurogenesis are conserved in the Drosophila larva CNS, a post-embryonic, juvenile stage which also harbors a BBB (Fig. 1A-B). The fly open circulatory system, powered by the cardiac tube, carries the hemolymph, which is in direct contact with all the organs including the CNS. The BBB represents its outermost structure. It is exclusively of glial nature, a property found in invertebrates but also in lower vertebrates, such as sharks (Bundgaard and Abbott, 2008), and is composed of two cell layers (Limmer et al., 2014; Stork et al., 2008). The subperineurial glia (SPG) are large polarised cells forming an epithelium-like structure with septate junctions (Fig. 1C), the equivalent of tight junctions in vertebrates. These represent a physical barrier to paracellular diffusion, similarly to the mammalian brain vascular endothelium (Hindle and Bainton, 2014; Weiler et al., 2017). The perineurial glia (PG), which does not have septate junctions, covers the SPG and is proposed to be a hemolymph sensor (DeSalvo et al., 2011; Parkhurst et al., 2018). Transcriptional analysis of the SPG and PG layers uncovered a striking conservation of molecules with mouse BBB cells, including transporters and cell adhesion molecules (DeSalvo et al., 2014). A recent study has confirmed the relevance of the fly model,

showing shared mechanisms of response to xenobiotics (Hindle et al., 2017). Thus, the Drosophila BBB represents a physical and chemical barrier that retains conserved chemoprotective strategies with the mammalian BBB, ensuring brain homeostasis and protecting the brain from toxins and pathogens (Mayer et al., 2009).

Here we show that the Drosophila larval brain is a relevant and valuable system to model brain infection and discover cellular mechanisms of BBB crossing by mammalian pathogens. Taking advantage of this innovative model, we identified Blr, a lipoprotein displaying leucine rich repeat domains similar to those found in the internalin A of *Listeria monocytogenes*, as a new virulence factor contributing to GBS neurotropism from fly to mouse. We further identify the Drosophila lipoprotein receptor LpR2 as a putative receptor for Blr in the BBB, mediating GBS internalisation.

Results

Group B Streptococcus actively invades the Drosophila larval brain in an explant set up.

Establishing a model of brain infection in the fly larva required developing experimental set-ups in which whole, intact living brains would be in contact with selected pathogens. We first devised an *ex vivo* protocol, as a straightforward, versatile platform for screening pathogens and conditions (Fig. 1D). Whole third instar larvae were opened posteriorly to expose all tissues while preventing damages to the brain and minimising injuries of the peripheral nerves. These brain explants, (including all larval tissues minus the gut, see Materials and Methods) were transferred to culture conditions that preserve cell viability, cell proliferation and BBB permeability (Supplementary Fig. 1A-D). In these conditions, brain explants could be kept for up to 48 h, at 30 °C. The culture medium was then inoculated with selected pathogens at selected doses (see Materials and methods). Brain explants were left in contact with pathogens for a given time (usually 3 h) to allow binding, washed several times to remove unattached microorganisms and kept in culture until the desired time of analysis. Whole fixed brains were scanned via confocal microscopy, allowing precise localisation and quantification of individual pathogens to assess brain entry and distinguish it from adhesion.

We used this set-up to screen for prokaryotic or eukaryotic pathogens known to trigger encephalitis and/or meningitis in mammals. We found that several were able to cross the Drosophila BBB and generate brain infection 24 h after inoculation (*Streptococcus agalactiae*, *Streptococcus pneumoniae*, *Neisseria meningitidis*, *Listeria monocytogenes* and *Candida glabrata*; Supp. Fig. 1E). In contrast, non-pathogenic strains (*Lactobacillus plantarum*, non-

pathogenic *Escherichia coli*, and *Saccharomyces cerevisiae*) were not able to enter the Drosophila brain, pointing to specific entry mechanisms under these conditions. Amongst the various pathogens tested, *S. agalactiae (*Group B Streptococcus, GBS*)* proved to be the most efficient to cross the fly BBB and it was detected both inside the brain and attached to its surface (Fig. 1E). We thus focused on GBS.

GBS is an opportunistic gram-positive bacterium responsible for severe invasive infections in neonates developing in pneumonia, septicaemia and meningitis (Doran and Nizet, 2004; Rajagopal, 2009; Shabayek and Spellerberg, 2018). Despite available antibiotic treatments and intrapartum prophylaxis, these cases still represent 10% of mortality and neurological sequelae in 25 to 50% of survivors, including cognitive impairment, seizures, hearing loss, and blindness (Libster et al., 2012; Schuchat, 1999). Among the various GBS clinical isolates tested, NEM316 was the most efficient to infect Drosophila larval brain explants, and chosen as our reference GBS strain (Fig. 1F, from now on called GBS). Interestingly, dead, formaldehyde-fixed GBS, in which surface structures cannot be rearranged, were unable to enter Drosophila brain explants, underlining the existence of an active mechanism for GBS entry.

The capacity of GBS to cause meningitis and ultimately neurological sequelae is linked to its ability to cross the BBB and invade the brain (Dando et al., 2014; Shabayek and Spellerberg, 2018). We first assayed BBB permeability of brain explants by dextran diffusion (see Materials and methods), and found that it was significantly increased during GBS infection (Fig. 2A). We also noticed, in some cases, an altered morphology of SPG membrane and septate junctions, as assessed by the use of specific markers at confocal microscopy resolution (Supp. Fig. 2A-B). These changes in BBB parameters were not particularly associated with GBS localisation, but rather brain-wide, suggesting a systemic origin. Interestingly, extracellular acidosis has been shown to build in the brain under meningitis (Andersen et al., 1989; Eross et al., 1981), and GBS is known to secrete lactic acid and acidify the culture environment (Libster et al., 2012). Measuring the pH of the culture medium at 3 h post infection actually revealed a strong acidification (Supp. Fig. 2C). To assess the contribution of acidification to GBS infection, we buffered the cultured medium with HEPES. Blocking medium acidification strongly prevented the increase in BBB permeability observed under infection by wild-type GBS (Fig. 2A), and restored BBB and septate junction morphologies (Fig. 2B-C and Supp. Fig. 2A-B). Bacterial counts in the brain also significantly changed, however moderately, in buffered medium compared to non-buffered (Fig. 2D). Furthermore we detected bacteria attached to the brain surface through scanning electron microscopy in both conditions (SEM, Fig. 2E). Altogether

these data showed that, although acidification might help GBS by altering BBB features, it is not absolutely required or essential for GBS entry in the brain. This argues for the involvement of specific mechanisms for BBB crossing by GBS.

The B Streptoccocal surface lipoprotein Blr is required for BBB crossing.

To identify GBS surface component(s) involved in this process, we first tested known factors implicated in pathogen virulence and adhesion to endothelial cells (Fig. 2F), such as the polysaccharide capsule (acapsular mutant Δ*cpsE*), the hemolytic lipid toxin (non-hemolytic strain Δ*cylE* and hyper-hemolytic strain *cyl*+), or cell-wall anchored proteins (Δ*srtA*). None of these mutants were significantly impaired in BBB crossing (Suppl. Fig. 2D). We thus tested the contribution of lipoproteins which are tethered to the cell membrane by an N-terminal lipid moiety. In Gram$^+$ bacteria, lipoprotein biosynthesis involves two specific enzymes, i) Lgt (prolipoprotein diacylglyceryl transferase), which attaches the lipid anchor to the prolipoproteins and ii) Lsp (lipoprotein signal peptidase), which specifically removes the N-terminal signal peptide of fully mature lipoproteins. In our model, removing either Lgt or Lsp decreased bacterial count within the brain at 24 h post infection, and the double mutant (Δ*lgt/lsp*) displayed an additive drop (Fig. 2G), leading to a strong impairment in GBS brain entry. GBS translocation into the brain was next assessed at earlier time points and a significant decrease was also demonstrated at 6 h post-infection for *Δlgt/lsp* mutants (Fig. 2H).

Next, we sought to identify specific GBS lipoprotein(s) involved in BBB crossing. The GBS repertoire consists of 39 putative GBS lipoproteins (C. Sutcliffe and J. Harrington, 2004), most of them being substrate binding proteins of ATP-binding cassette (ABC) transporters. We selected Blr (group B leucine rich) protein, as an interesting candidate. Blr is a His-triad/Leucine Rich Repeat (LRR) protein related to the internalin A (InlA) of *Listeria monocytogenes*, a surface protein crucial for bacterial crossing of gut and brain barriers. Both InlA and Blr contain LRR domains, classically associated with protein-protein interaction and ligand recognition (Kobe and Kajava, 2001; Waldemarsson et al., 2006). To test the role of *blr* (annotated as *gbs0918*), we deleted the gene in GBS NEM316. We first checked that GBS NEM316 and its isogenic mutants grew similarly in various rich laboratory media (THY, BHI) at 37 °C and in Drosophila Schneider medium at 30 °C supplemented or not with HEPES (Suppl. Fig. 2E), ruling out any effect due to growth defect. Moreover, using SEM, we found no obvious difference in morphology between WT and *Δblr*, that we found attached to the brain surface and in chains (Fig. 2I-J). However, as shown in Fig. 2G, *Δblr* displayed a significant

decrease in bacterial count in the Drosophila larval brain at 24 h post infection compared to the control wild-type and complemented (*Δblr+blr*) strains. GBS translocation into the brain was also significantly decreased at 6 h post-infection for Δ*blr* mutants (Fig. 2H). Altogether, these results showed that GBS lipoproteins, and in particular Blr, are key contributors to cross the Drosophila larval BBB and enter the brain *ex vivo*.

Surprisingly, we noticed that infection by Δ*blr* mutants resulted in significant damages to SPG membranes, altered septate junction architecture and increased BBB permeability compared to wild-type GBS (Supp. Fig. 2A-B and Supp. Fig. 3A). These differences were decreased but still remained when culture medium pH was maintained (Supp. Fig. 2A-B and Supp. Fig. 3A), and acidification was similar regardless of the bacterial strain (Supp. Fig. 2C), ruling out a differential effect from acidosis. Of note, none of these features were observed with the double Δ*lgt/lsp* mutant (Supp. Fig. 2A-B and Supp. Fig. 3A). In addition, using SEM, we noticed the presence of additional, large structures reminiscent of the polysaccharidic coat produced during biofilm formation (Supp. Fig. 3B). Altogether, these data suggest that, in the absence of Blr, GBS turns on more destructive, yet much less efficient alternative mechanisms dependent on other lipoproteins. They also point to specific Blr-dependent mechanisms for GBS attraction to and crossing of the BBB.

The Drosophila lipoprotein receptor LpR2 is essential in the BBB for brain invasion by GBS

We then wondered how the lipoprotein Blr overcomes the physical barrier of the SPG (Fig. 1A). Interestingly, the LRR-containing InlA was shown to interact with human E-cadherin (Lecuit et al., 1997) that is is highly conserved in flies. We tested the role of E-cadherin in GBS entry *ex vivo*, and found that specifically knocking it down in the SPG layer, through the GAL4/UAS system (Brand and Perrimon, 1993), did not affect GBS brain entry (Fig. 3A). This suggests that GBS does not rely on E-cadherin for entering the brain.

Lipoprotein receptors are conserved throughout the animal kingdom, and were originally identified as surface receptors capable of mediating cellular lipid uptake, (Dieckmann et al., 2010). Lipids circulate in the blood in association with specific proteins called apolipoproteins (apo), forming lipoprotein particles of different densities (Low Density, LDL; Very Low density, VLDL). Lipoprotein receptors can be classified in two main groups, based on whether they behave as endocytic receptors supporting lipoprotein internalisation (LDLR, VLDLR, SR-A) or as mediators of lipid exchange at the cell surface. Of interest, Drosophila lipoproteins and lipoprotein receptors are similar to those in vertebrates (Palm et al., 2012; Parra-Peralbo and

Culi, 2011). Drosophila has seven lipoprotein receptors, belonging to the (V)LDLR families. Interestingly, specific lipoprotein particles were shown to cross the larval BBB, which express receptors LRP1 and Megalin (Brankatschk and Eaton, 2010; Brankatschk et al., 2014; DeSalvo et al., 2011).

We investigated which lipoprotein receptors were expressed on the SPG, and if they could be important for GBS entry. Transcriptional data suggested expression of LpR1, LpR2, Arr and Mgl in the SPG (*Pauline Spéder and Andrea H. Brand, unpublished data*). Specific knockdown of these receptors identified LpR2 as the main lipoprotein receptor mediating GBS entry in the brain (Fig. 3A). More precisely, knocking down LpR2 in the SPG only was sufficient to decrease GBS count in the brain at 24 h post infection. Using a gene knock-in producing an endogenous LpR2-GFP fusion (LpR2::GFP MiMIC line), we observed that LpR2 expression was restricted to the SPG, where it colocalised with a membrane marker (Fig. 3B). Similar results were obtained using an anti-LpR2 antibody (Supp. Fig. 3C-D''). These results show that LpR2, a lipoprotein receptor specifically expressed in the SPG, is crucial for GBS dissemination into the brain.

GBS surface lipoprotein Blr binds to the Drosophila LpR2, allowing endocytosis-dependent transcellular crossing of the BBB

Interestingly, LpR2 has been shown to be an endocytic receptor, able to mediate the uptake of lipoprotein particles (Parra-Peralbo and Culi, 2011; Rodríguez-Vázquez et al., 2015). We hypothesised that binding of LpR2 to Blr could first help GBS adhere to the BBB, and ultimately lead to its internalisation into the SPG through endocytosis.

We first tested if LpR2 and Blr were able to physically interact. We set up a co-immunoprecipitation experiment between the two species, incubating bacterial lysate on Lpr2-GFP fusions extracted from larval brains and bound to beads (see Materials and Methods). We showed that Blr was found in the bacterial eluates from Lpr2-GFP beads for wild-type and complemented Δ*blr*+*Blr* strains, whereas no band was recovered from Δ*blr* eluates (Fig. 3C and Supp. Fig. 3E). These data showed that Drosophila LpR2 is able to bind streptococcal Blr.

We further assessed the role of the endocytic pathway in GBS entry. We blocked endocytosis specifically in the SPG by preventing dynamin (Drosophila Shibire) function through the overexpression of temperature-sensitive (*shibire*^{ts}) or dominant-negative (*shibire*^{DN}) non-functional forms. This led to a strong decrease in bacterial counts within the brain, detected as early as 6 h post-infection (Fig. 3D). In addition, we infected larval brains in which a marker for early endosomes (Rab5-GFP) was ubiquitously expressed along a specific marker for the

SPG membrane. Under these conditions we were able to detect GBS in vesicles co-staining for Rab5-GFP and SPG membranes (Fig. 3E). Expressing another early endocytic marker (FYVE-GFP) specifically in the SPG gave similar results (Supp. Fig. 3F). Finally, we were able to detect GBS in lysosomal vesicles coming from the SPG layer, through the specific expression of the Lamp1-GFP marker (Fig. 3F). Taken together, these results strongly indicate that BBB crossing by GBS occurs via endocytosis, likely through binding of Blr to LpR2 and internalisation of the resulting complexes.

GBS uses a panel of strategies to enter the brain .

So far, we focused on the mechanisms allowing GBS invasion of the brain and access to the parenchyma through crossing of the physical component of the BBB harbouring cellular junctions, the SPG. However the BBB is a composite structure, with additional protective layers. GBS has first to overcome a layer of extracellular matrix and then the PG (Fig. 1A-B). Indeed, we found that the presence of GBS on the surface of the brain colocalised with an absence of staining for collagen IV, a major, conserved ECM component of the extracellular matrix (Fig. 4A-B). Interestingly, GBS displays lytic activity on a collageno-mimetic peptide (Jackson et al., 1994). This could pinpoint that GBS destroys the ECM to gain access to the cellular layers. GBS would then encounter the PG, which does not harbour intercellular junctions, as the first cellular layer. Interestingly, we found that neither lipoprotein receptors nor E-cadherin were required in this layer for GBS brain entry (Fig. 4C), and blocking endocytosis in the PG did not alter brain invasion (Supp. Fig. 4). Moreover, we observed that the PG structure seemed altered (Fig. 4D-E). Taking these data together, we propose that rupture of the ECM through GBS collagenolytic activity precedes the bacterial traversal of the PG layer, through paracellular or destructive mechanisms. Blr could then bind to LpR2 on the surface of the SPG allowing GBS endocytosis and brain invasion.

Blr is a virulence factor essential for BBB crossing in the Drosophila larva.

This brain explant protocol in the Drosophila larva led us to uncover and propose a novel mechanism for BBB crossing by GBS, in which the pathogen surface lipoprotein Blr interacts with the host lipoprotein receptor LpR2, leading to bacterial endocytosis and CNS invasion.
To confirm these findings in an *in vivo* set-up, we developed a protocol of brain infection through pathogen microinjection into the Drosophila circulatory system (Fig. 5A). It was

preferred to feeding in order to control the dose and bypass the variability in gut crossing efficiency.

Bacterial counts in the brain of surviving larvae at 4 h and 18 h post injection revealed that GBS was able to access and enter the Drosophila brain via the systemic route (Fig. 5B and Supp. Fig. 5A). Survival curves (0 - 4 h post injection) showed that systemic infection by wild-type GBS increased larval lethality compared to mock injection (Fig. 5C). These results demonstrated that GBS is able to infect the Drosophila brain from a circulating, systemic route, causing animal mortality.

Next, we tested the virulence of Δ*lgt/lsp* and Δ*blr* mutants in this set-up. First, bacterial counts in the brains of surviving larvae injected with Δ*lgt/lsp* or Δ*blr* were significantly reduced compared to wild-type or complemented (Δ*blr*+*blr*) GBS strains at 4 h post injection (Fig. 5B). To discard differences in fitness or survival between these isogenic GBS strains, we determined through cfu (colony-forming units) counts (see Materials and Methods) the exact quantity of bacteria per animal: in or attached to the brain, in the hemolymph, and in all other solid tissues (Supp. Fig. 5B). We then calculated three ratios: brain to hemolymph, brain to tissues, brain to hemolymph and tissues (Supp. Fig. 5C). In all cases, we found a significant decrease in Δ*blr* ratios versus wild-type ratios. This shows that the loss of Blr specifically affects the neurotropic ability of GBS to adhere and/or enter the brain. In agreement with these results, survival scores were significantly higher in larvae injected with Δ*lgt/lsp* or Δ*blr* mutants compared to the two control strains, with a lethality level similar to non-infected animals (Fig. 5C).

We then assessed the role of LpR2 in the BBB during systemic infection. Infection by wild-type GBS of larvae in which LpR2 was specifically depleted in the SPG resulted in a dramatic reduction of bacterial count in the brain (Fig. 5D). Survival curves showed that depleting LpR2 in the SPG led to a delayed lethality compared to wild-type animals (compare black and dark orange curves in Fig. 5E), although it did not reach statistical significance. This suggests that, although lethality might result from brain infection, it likely also depends on a systemic effect.

Blr is a virulence factor essential for BBB crossing in mice.

Combining *ex vivo* and *in vivo* infection protocols allowed us to propose Blr as a virulence factor essential for brain invasion in Drosophila. To determine whether this mechanism is conserved in mammals, we used the mouse model of GBS hematogenous brain infection (Banerjee et al., 2011) and compared wild-type GBS strain with the isogenic *Δblr* mutant.

Time-course infection analysis showed that GBS could be detected in the brain as early as 3 h post-infection, was maintained at similar levels at 6 h and 24 h, and reduced at 48 h (Fig. 6A). In parallel, bacterial counts in the blood were measurable at 3 and 6 h post infection and dropped sharply at 24 h (Fig. 6B). Using a fluorescent GFP-tagged GBS, we observed bacteria attached to and in the capillaries of the brain parenchyma at 4 h post-infection (Fig. 6C, Supp. Fig. 6A) suggesting that the primary entry point for GBS is through the endothelial barrier. Interestingly, we were able to detect LDLR on these capillaries, underlying the availability of this receptor at GBS putative point of entry (Supp. Fig. 6B). Then, at 24 h after infection, we detected bacteria at the choroid plexuses and walls of the lateral (Fig. 6D), third, and fourth (not shown) ventricles, that also play a barrier role in the mammalian brain. Very few cells were detected in the brain parenchyma, in regions far from the ventricles, except for some small clusters in which typical streptococcal chains were identified.

Survival curves showed that infection with wild-type GBS led to more than 50% of lethality over 7 days (Fig. 6E). The mice that survived up to 7 days exhibited aberrant behavior indicative of neurological deficits, including unilateral palsy, immobilisation, and imbalance. Mood aberrations, such as isolation and lack of explorative behavior, were also observed. Moreover, the brains of these mice revealed meningitis hallmarks including meningeal thickening and leukocyte accumulation in the meninges compared with saline-injected control mice (Supp. Fig. 6C), as identified by co-staining for macrophages (CD68, pan-macrophage marker) and microglia (Iba-1, microglia/macrophage marker).

In contrast, no deaths were recorded in mice infected with *Δblr* mutants and their survival curve was significantly different compared to mice inoculated with wild-type GBS (Fig. 6E). We then analysed bacterial levels in the brain and in the blood over the course of infection. The levels of the Δ*blr* mutant in the blood were not significantly different from wild-type GBS neither at 3 h nor at 6 h post infection and we observed a similar clearance at 24 h (Supp. Fig. 6D). Importantly, the brain levels of the *Δblr* mutant at 3 h and at 6 h were lower, yet not significantly, and a significant reduction was observed at 24 h post-infection when compared with the wild-type strain (Supp. Fig. 6E). Normalising brain to blood levels confirmed that the Δ*blr* strain was significantly altered in its capacity to invade the mouse brain at 3 h and 6 h post infection, as compared to the wild-type (Fig. 6F).

Interestingly, none of the mice infected with the *Δlgt/lsp* mutant died, as observed with Δ*blr* mutants (Supp. Fig. 6F). Bacterial levels of *Δlgt*/*lsp* mutant were reduced both in the blood and brain compartments at 6 h post infection as compared to wild-type GBS (Supp. Fig. 6G). Yet,

the brain-to-blood ratios were not significantly different between these two strains (Supp. Fig. 6H) suggesting that *Δlgt/lsp* mutants are generally less fit *in vivo*.
Altogether these results identify Blr as a new, conserved virulence factor endowing GBS the ability to cross the BBB in Drosophila and mouse.

Discussion

Here we propose an original model of brain infection using the Drosophila larval brain, as a mean to investigate molecular and cellular mechanisms contributing to the crossing of the BBB. Amongst the various neurotropic pathogens tested in this model, Group B Streptococcus, a pathogen responsible for meningitis in neonates and immunocompromised adults, was the most efficient one and used herein. We were able to identify the surface lipoprotein Blr as a key contributor of GBS entry into the brain. Furthermore, we were able to show that Blr binds to Lpr2, a host lipoprotein receptor expressed in the Drosophila BBB. We propose that binding of Blr to Lpr2 promotes bacterial endocytosis, and GBS penetration into the brain through a transcellular passage (Fig. 7). Thus, using *in vivo* experiments in Drosophila, Blr and LprR2 were shown as key players in brain invasion. Blr contribution to CNS invasion was also established in a mouse model, demonstrating the power and relevance of the Drosophila model.

Our model combines an *ex vivo* approach with brain explants for straightforward, versatile and scalable screening of putative virulence factors and associated mechanisms, with a full *in vivo* approach to assess virulence and impact on the whole organism. Even though the *ex vivo* protocol does not allow to assess the contribution of circulating immune cells in BBB crossing, bypassing it can unveil BBB-specific mechanisms that could be masked either by an earlier, systemic effect (*e.g.*, general inflammation) or by the difficulty to detect or assess it (*e.g.*, acidosis). Interestingly, for example, *Cryptococcus neoformans* cannot enter the drosophila larval brain in the *ex vivo* conditions (Supp. Fig. 1E), a finding congruent with the contribution of the Trojan horse mechanism proposed to explain *C. neoformans* barrier crossing (Santiago-Tirado et al., 2017). It is worth noting that fly experiments were performed at 30°C, and not at 37°C, since 30°C is the maximal temperature allowing Drosophila development. Despite this temperature difference which can affect the expression of some virulence factors, several human neurotropic pathogens assayed here were able to invade the Drosophila larval brain.
Adult flies have been used previously as an infection model with GBS serotype Ia (A909 strain) through pricking, unveiling the role of GBS cell-wall anchored protein alpha C protein and host glycosaminoglycans as important for virulence and dissemination in the adult brain (Baron et

al., 2008; Chang et al., 2011). We chose to investigate the larval brain in order to study the impact of infection in a developing brain, where extensive neurogenesis is happening and neural circuits are being established, mimicking more closely neonatal infections caused by GBS.

Using our model, we demonstrated the key contribution of surface-exposed lipoproteins in mediating entry of GBS into the drosophila larval brain and then pinpointed the role of a specific lipoprotein known as Blr (for group B leucine rich) in a seemingly seamless fashion, through direct binding to the host lipoprotein receptor LpR2 expressed on the Drosophila BBB. We focused our attention on Blr as an attractive candidate, because its surface exposed LRR region composed of 12.5 repeats of 22 amino acids, which is highly similar to LRR region of internalin A (InlA) of *L. monocytogenes*, one of the best studied pathogenic bacteria (Mengaud et al., 1996). Blr was shown to be expressed *in vivo* but camouflaged by the bacterial capsule. No role in virulence had been attributed to Blr yet. Indeed, Blr had been studied following intraperitoneal infection in a mouse model that bypasses the initial adhesion step. Interestingly though, it was shown that Blr can bind to the Pathogen Recognition Receptor SR-A (scavenger receptor A) expressed on most macrophages, and known to bind and endocytose modified low-density lipoproteins (Areschoug et al., 2008). This finding strongly supports our findings that Blr interacts with a specific lipoprotein receptor Lpr2 and is then internalised through endocytosis in the Drosophila SPG.

Thus, GBS takes advantage of a host receptor expressed in the BBB as one strategy to cross this barrier. The physiological role of LpR2 in the BBB has not been described. In other tissues, LpR2, as well as the closely related LpR1, have been implicated in lipid metabolism (Parra-Peralbo and Culi, 2011; Rodríguez-Vázquez et al., 2015). Whole mutants for LpR2 and LpR1 are actually viable, suggesting that these receptors are not essential at least under homeostatic conditions.

During GBS infection, some bacterial lipoproteins are released in the extracellular environment and bind TLR2 through their lipid moiety (Henneke et al., 2008). However endogenous lipoprotein receptors, which are the natural receptor for lipoproteins *in vivo*, have been shown to bind lipoprotein complexes through their protein component (apolipoprotein) (Blacklow, 2007). In addition, it is known that lipoprotein receptors bind most of their ligands through clusters of cysteine-rich LDL receptor type-A (LA) modules. LpR2, which bears between 7 and 9 LA motifs depending on the isoform (Parra-Peralbo and Culi, 2011), could thus bind Blr through its protein moiety. The LRR domain (Fig. 2F') would be of specific interest. Blr is also a virulence factor critical for BBB crossing in mice. Lpr2 is orthologous to both LDLR and

VLDLR proteins. Both LDLR and VLDLR have been shown to be expressed in brain endothelial cells, where they are linked to the uptake of molecular complexes across the BBB (Deane et al., 2008; Molino et al., 2017; Pan et al., 2004). Here we confirmed LDLR localisation in blood vessels on the mouse brain *in situ* (Supp. Fig. 6B). Interestingly, VLDLR has been implicated in mediating the entry of Hepatitis C Virus into host cells through endocytosis (Ujino et al., 2016). The targeting of endogenous lipoprotein receptors could thus be a conserved strategy shared by a diversity of pathogens to enter cells and ultimately cross barriers, including the BBB.

Of note, we found that GBS acidifies the extracellular environment, a known parameter during meningitis. Although we demonstrated that it is not required for BBB crossing by GBS, it might help bacterial invasion, at least on a longer term, by weakening the SPG and/or affecting other layers. Indeed, lactic acid has been proposed as a virulence factor in rat fetal lung explants, where it is linked to tissue destruction (Kling et al., 2009). Interestingly, we noticed destroyed blood capillaries in the brain of mice infected with wild-type GBS (Supp. Fig. 6A), as well as brains with highly altered SPG during infection by wild-type GBS in our *in vivo* Drosophila model (data not shown). This suggests that acidosis-linked alteration of the BBB might be a conserved mechanism taking place during genuine infection.
Interestingly, Blr-deficient bacteria were less able to enter the brain while causing higher damages of the SPG. As mentioned previously, this suggests that when Blr is not available at their surface, bacteria turn to an alternative pathway, less efficient but more destructive, perhaps to gain access through alteration of junctions and tissue integrity. Such damages are not seen under infection with lipoprotein-deficient bacteria, in which GBS brain entry is extremely low. This indicates first that other lipoproteins support such a pathway, and also could explain why Δ*blr* still enters better than Δ*lgt/lsp*. The presence of biofilm is intriguing, and could be a way Δ*blr* mutants cause additional damage to the BBB. Altogether, these different results underline the ability of GBS to shapeshift and use different mechanisms independently or together, depending on the conditions.

In conclusion, we propose the following model for GBS entry into the fly larval brain: rupture of the ECM through GBS collagenolytic activity and then traversal of the PG layer, through paracellular or destructive mechanisms. Then Blr comes at play, binds to LpR2 on the surface of the SPG allowing GBS endocytosis and brain invasion (Fig. 7). Our work, using an original model of brain infection in Drosophila, thus proposes a detailed mechanism behind pathogen crossing of the complex BBB structure, and identifies the specific lipoprotein Blr as a new

virulence factor for GBS. Ultimately, understanding the exact cellular and molecular pathways employed by pathogens to use and corrupt the physiological role of host receptors will provide new insight into means of helping the BBB to restrict pathogen entry during infection as well as bypassing this barrier to target therapeutics molecules.

Author Contributions

B.B. performed most Drosophila experiments. N.R. generated Fig. 2F, Fig. 3C, Supp. Fig. 7A and parts of Fig. 3D and Fig. 4A under the supervision of B.B. P.S. devised the brain explant protocol and started the pathogen screen. B.B. and P.S. designed and analysed all Drosophila experiments. B.P. and S.D. generated GBS strains and constructs as well as performed growth curves. S.D. designed and advised on all GBS experiments. F.P. designed, performed and analysed, together with K.S., the mouse experiments and generated Fig. 6 and Supp. Fig. 6. V.M. provided consultation on the mouse infection model and resources. R.M. supervised and advised on all mouse experiments and analysis. B.B., S.D. and P.S. wrote the article with input from FP and RM.

Acknowledgments

We are deeply grateful to C. Schmitt and the Ultrastructure UTechS Ultrastructural Bioimaging platform of the Institut Pasteur for their expertise and support in SEM and EM. We thank J. Culi, C. d'Enfert, G. Janbon, F. Leulier, M-K. Taha, M. Lecuit, F. Schweisguth, and G. Waldemarsson for reagents and strains. We are very grateful to Gunnar Lindahl for the kind gift of his homemade antibody against Blr lipoprotein. L. Arbogast generated the *mdr65-mtdt-Tomato* construct. Stocks obtained from the Bloomington Drosophila Stock Center (NIH P40OD018537) and from the Vienna Drosophila Resource Center were used in this study. We are extremely grateful to A-E. Deghmane, O. Disson, C. d'Enfert, G. Janbon, M-K. Taha and M. Lecuit for their kind and enthusiastic help and advice with the pathogen screen. We are indebted to D. Ferrandon for his expert advice on the project and to S. Liégeois for technical help, especially introducing us to hemolymph injection of Drosophila larvae. We thank B. Montagne for help with the Western blots. We thank E. Voulgari for valuable advice and S. Trygoni and D. Dionysopoulou for technical support on the mouse infection model. Further, we are grateful to the personnel of the Department of Animal Models for Biomedical Research of the Hellenic Pasteur Institute for their invaluable help. We thank D. Ferrandon for critical reading of the manuscript. This work has been funded by a starting package from Institut Pasteur/ Labex Revive and a JCJC grant from Agence Nationale de la Recherche (NeuraSteNic, ANR- 17-CE13-0010-01) to P.S.; a Grand Projet Fédérateur Microbes & Brains InFeSteR grant from Institut Pasteur to P.S., R.M. and S.D. B.B. has been supported by a Roux-Cantarini and a Labex Revive post-doctoral fellowships.

References

Andersen, N.E.O., Gyring, J., Hansen, A.J., Laursen, H., and Siesjö, B.K. (1989). Brain Acidosis in Experimental Pneumococcal Meningitis. J. Cereb. Blood Flow Metab. *9*, 381–387.

Areschoug, T., Waldemarsson, J., and Gordon, S. (2008). Evasion of macrophage scavenger receptor A-mediated recognition by pathogenic streptococci. Eur. J. Immunol. *38*, 3068–3079.

Banerjee, A., Kim, B.J., Carmona, E.M., Cutting, A.S., Gurney, M.A., Carlos, C., Feuer, R., Prasadarao, N. V., and Doran, K.S. (2011). Bacterial Pili exploit integrin machinery to promote immune activation and efficient blood-brain barrier penetration. Nat. Commun. *2*, 462.

Banks, W. a (2012). Brain meets body: the blood-brain barrier as an endocrine interface. Endocrinology *153*, 4111–4119.

Baron, M.J., Wong, S.L., Nybakken, K., Carey, V.J., and Madoff, L.C. (2008). Host Glycosaminoglycan Confers Susceptibility to Bacterial Infection in Drosophila melanogaster. Infect. Immun. *77*, 860–866.

Bergman, P., Seyedoleslami Esfahani, S., and Engström, Y. (2017). Drosophila as a Model for Human Diseases—Focus on Innate Immunity in Barrier Epithelia. Curr. Top. Dev. Biol. *121*, 29–81.

Bergmann, S., Lawler, S.E., Qu, Y., Fadzen, C.M., Wolfe, J.M., Regan, M.S., Pentelute, B.L., Agar, N.Y.R., and Cho, C.-F. (2018). Blood–brain-barrier organoids for investigating the permeability of CNS therapeutics. Nat. Protoc. *13*, 2827–2843.

Bier, E., and Guichard, A. (2012). Deconstructing host-pathogen interactions in Drosophila. Dis. Model. Mech. *5*, 48–61.

Blacklow, S.C. (2007). Versatility in ligand recognition by LDL receptor family proteins: advances and frontiers. Curr. Opin. Struct. Biol. *17*, 419–426.

Brand, A.H., and Perrimon, N. (1993). Targeted gene expression as a means of altering cell fates and generating dominant phenotypes. Development *118*, 401–415.

Brankatschk, M., and Eaton, S. (2010). Lipoprotein particles cross the blood-brain barrier in Drosophila. J. Neurosci. *30*, 10441–10447.

Brankatschk, M., Dunst, S., Nemetschke, L., and Eaton, S. (2014). Delivery of circulating lipoproteins to specific neurons in the Drosophila brain regulates systemic insulin signaling.

Elife *3*, 1–19.

Bundgaard, M., and Abbott, N.J. (2008). All vertebrates started out with a glial blood-brain barrier 4-500 million years ago. Glia *56*, 699–708.

C. Sutcliffe, I., and J. Harrington, D. (2004). Putative lipoproteins of Streptococcus agalactiae identified by bioinformatic genome analysis. Antonie Van Leeuwenhoek *85*, 305–315.

Cain, M.D., Salimi, H., Diamond, M.S., and Klein, R.S. (2019). Mechanisms of Pathogen Invasion into the Central Nervous System. Neuron *103*, 771–783.

Chang, Y.-C., Wang, Z., Flax, L.A., Xu, D., Esko, J.D., Nizet, V., and Baron, M.J. (2011). Glycosaminoglycan binding facilitates entry of a bacterial pathogen into central nervous systems. PLoS Pathog. *7*, e1002082.

Coureuil, M., Lécuyer, H., Bourdoulous, S., and Nassif, X. (2017). A journey into the brain: insight into how bacterial pathogens cross blood–brain barriers. Nat. Rev. Microbiol. *15*, 149–159.

Dando, S.J., Mackay-Sim, A., Norton, R., Currie, B.J., St John, J. a, Ekberg, J. a K., Batzloff, M., Ulett, G.C., and Beacham, I.R. (2014). Pathogens penetrating the central nervous system: infection pathways and the cellular and molecular mechanisms of invasion. Clin. Microbiol. Rev. *27*, 691–726.

Daneman, R. (2012). The blood-brain barrier in health and disease. Ann. Neurol. *72*, 648–672.

Daneman, R., and Prat, A. (2015). The Blood – Brain Barrier. 1–24.

Deane, R., Sagare, A., Hamm, K., Parisi, M., Lane, S., Finn, M.B., Holtzman, D.M., and Zlokovic, B. V (2008). apoE isoform-specific disruption of amyloid beta peptide clearance from mouse brain. J. Clin. Invest. *118*, 4002–4013.

DeSalvo, M.K., Mayer, N., Mayer, F., and Bainton, R.J. (2011). Physiologic and anatomic characterization of the brain surface glia barrier of Drosophila. Glia *59*, 1322–1340.

DeSalvo, M.K., Hindle, S.J., Rusan, Z.M., Orng, S., Eddison, M., Halliwill, K., and Bainton, R.J. (2014). The Drosophila surface glia transcriptome: evolutionary conserved blood-brain barrier processes. Front. Neurosci. *8*, 346.

Dieckmann, M., Dietrich, M.F., and Herz, J. (2010). Lipoprotein receptors--an evolutionarily ancient multifunctional receptor family. Biol. Chem. *391*, 1341–1363.

Disson, O., and Lecuit, M. (2013). In vitro and in vivo models to study human listeriosis:

mind the gap. Microbes Infect. *15*, 971–980.

Doran, K.S., and Nizet, V. (2004). Molecular pathogenesis of neonatal group B streptococcal infection: no longer in its infancy. Mol. Microbiol. *54*, 23–31.

Doran, K.S., Banerjee, A., Disson, O., and Lecuit, M. (2013). Concepts and mechanisms: Crossing host barriers. Cold Spring Harb. Perspect. Med. *3*.

Eross, J., Silink, M., and Dorman, D. (1981). Cerebrospinal fluid lactic acidosis in bacterial meningitis. Arch. Dis. Child. *56*, 692–698.

Ferrandon, D. (2013). The complementary facets of epithelial host defenses in the genetic model organism Drosophila melanogaster: from resistance to resilience. Curr. Opin. Immunol. *25*, 59–70.

Heidari, H., and Taylor, H. (2018). Review Article: Capturing the physiological complexity of the brain's neuro-vascular unit *in vitro*. Biomicrofluidics *12*, 051502.

Henneke, P., Dramsi, S., Mancuso, G., Chraibi, K., Pellegrini, E., Theilacker, C., Hübner, J., Santos-Sierra, S., Teti, G., Golenbock, D.T., et al. (2008). Lipoproteins are critical TLR2 activating toxins in group B streptococcal sepsis. J. Immunol. *180*, 6149–6158.

Hindle, S.J., and Bainton, R.J. (2014). Barrier mechanisms in the Drosophila blood-brain barrier. Front. Neurosci. *8*, 414.

Hindle, S.J., Munji, R.N., Dolghih, E., Jacobson, M.P., Daneman, R., Bainton, R.J., Gaskins, G., Orng, S., Ishimoto, H., Soung, A., et al. (2017). Evolutionarily Conserved Roles for Blood-Brain Barrier Xenobiotic Transporters in Endogenous Steroid Partitioning and Behavior. Cell Rep. *21*, 1304–1316.

Jackson, S., Meeks, C., Vézina, A., Robey, R.W., Tanner, K., and Gottesman, M.M. (2019). Model systems for studying the blood-brain barrier: Applications and challenges. Biomaterials *214*, 119217.

Kling, D.E., Cavicchio, A.J., Sollinger, C.A., Madoff, L.C., Schnitzer, J.J., and Kinane, T.B. (2009). Lactic acid is a potential virulence factor for group B Streptococcus. Microb. Pathog. *46*, 43–52.

Kobe, B., and Kajava, A. V (2001). The leucine-rich repeat as a protein recognition motif. Curr. Opin. Struct. Biol. *11*, 725–732.

Kristensson, K. (2011). Microbes' roadmap to neurons. Nat. Rev. Neurosci. *12*, 345–357.

Lampron, A., ElAli, A., and Rivest, S. (2013). Innate Immunity in the CNS: Redefining the

relationship between the CNS and its Environment. Neuron *78*, 214–232.

Lecuit, M., Ohayon, H., Braun, L., Mengaud, J., and Cossart, P. (1997). Internalin of Listeria monocytogenes with an intact leucine-rich repeat region is sufficient to promote internalization. Infect. Immun. *65*, 5309–5319.

Lemaitre, B., and Hoffmann, J. (2007). The Host Defense of *Drosophila melanogaster*. Annu. Rev. Immunol. *25*, 697–743.

Libster, R., Edwards, K.M., Levent, F., Edwards, M.S., Rench, M.A., Castagnini, L.A., Cooper, T., Sparks, R.C., Baker, C.J., and Shah, P.E. (2012). Long-term Outcomes of Group B Streptococcal Meningitis. Pediatrics *130*, e8–e15.

Limmer, S., Weiler, A., Volkenhoff, A., Babatz, F., and Klämbt, C. (2014). The Drosophila blood-brain barrier: development and function of a glial endothelium. Front. Neurosci. *8*, 365.

Liu, Y., Gordesky-Gold, B., Leney-Greene, M., Weinbren, N.L., Tudor, M., and Cherry, S. (2018). Inflammation-Induced, STING-Dependent Autophagy Restricts Zika Virus Infection in the Drosophila Brain. Cell Host Microbe *24*, 57-68.e3.

Mayer, F., Mayer, N., Chinn, L., Pinsonneault, R.L., Kroetz, D., and Bainton, R.J. (2009). Evolutionary conservation of vertebrate blood-brain barrier chemoprotective mechanisms in Drosophila. J. Neurosci. *29*, 3538–3550.

Mengaud, J., Ohayon, H., Gounon, P., Mege, R.M., and Cossart, P. (1996). E-cadherin is the receptor for internalin, a surface protein required for entry of *L. monocytogenes* into epithelial cells. Cell *84*, 923–932.

Molino, Y., David, M., Varini, K., Jabès, F., Gaudin, N., Fortoul, A., Bakloul, K., Masse, M., Bernard, A., Drobecq, L., et al. (2017). Use of LDL receptor–targeting peptide vectors for *in vitro* and *in vivo* cargo transport across the blood-brain barrier. FASEB J. *31*, 1807–1827.

Obermeier, B., Daneman, R., and Ransohoff, R.M. (2013). Development, maintenance and disruption of the blood-brain barrier. Nat. Med. *19*, 1584–1596.

Palm, W., Sampaio, J.L., Brankatschk, M., Carvalho, M., Mahmoud, A., Shevchenko, A., and Eaton, S. (2012). Lipoproteins in Drosophila melanogaster--assembly, function, and influence on tissue lipid composition. PLoS Genet. *8*, e1002828.

Pan, W., Kastin, A.J., Zankel, T.C., van Kerkhof, P., Terasaki, T., and Bu, G. (2004). Efficient transfer of receptor-associated protein (RAP) across the blood-brain barrier. J. Cell Sci. *117*, 5071–5078.

Parkhurst, S.J., Adhikari, P., Navarrete, J.S., Legendre, A., Manansala, M., and Wolf, F.W. (2018). Perineurial Barrier Glia Physically Respond to Alcohol in an Akap200-Dependent Manner to Promote Tolerance. Cell Rep. *22*, 1647–1656.

Parra-Peralbo, E., and Culi, J. (2011). Drosophila lipophorin receptors mediate the uptake of neutral lipids in oocytes and imaginal disc cells by an endocytosis-independent mechanism. PLoS Genet. *7*.

Péan, C.B., and Dionne, M.S. (2014). Intracellular infections in Drosophila melanogaster: host defense and mechanisms of pathogenesis. Dev. Comp. Immunol. *42*, 57–66.

Rajagopal, L. (2009). Understanding the regulation of Group B Streptococcal virulence factors. Future Microbiol. *4*, 201–221.

Rodríguez-Vázquez, M., Vaquero, D., Parra-Peralbo, E., Mejía-Morales, J.E., and Culi, J. (2015). Drosophila Lipophorin Receptors Recruit the Lipoprotein LTP to the Plasma Membrane to Mediate Lipid Uptake. PLOS Genet. *11*, e1005356.

Santiago-Tirado, F.H., Onken, M.D., Cooper, J.A., Klein, R.S., and Doering, T.L. (2017). Trojan Horse Transit Contributes to Blood-Brain Barrier Crossing of a Eukaryotic Pathogen. MBio *8*.

Saunders, N.R., Habgood, M.D., Møllgård, K., and Dziegielewska, K.M. (2016). The biological significance of brain barrier mechanisms: help or hindrance in drug delivery to the central nervous system? F1000Research *5*.

Schuchat, A. (1999). Group B streptococcus. Lancet *353*, 51–56.

Shabayek, S., and Spellerberg, B. (2018). Group B Streptococcal Colonization, Molecular Characteristics, and Epidemiology. Front. Microbiol. *9*, 437.

Siegenthaler, J. a, Sohet, F., and Daneman, R. (2013). “Sealing off the CNS”: cellular and molecular regulation of blood-brain barriergenesis. Curr. Opin. Neurobiol. 1–8.

Sivandzade, F., and Cucullo, L. (2018). In-vitro blood–brain barrier modeling: A review of modern and fast-advancing technologies. J. Cereb. Blood Flow Metab. *38*, 1667–1681.

Stork, T., Engelen, D., Krudewig, A., Silies, M., Bainton, R.J., and Klämbt, C. (2008). Organization and function of the blood-brain barrier in Drosophila. J. Neurosci. *28*, 587–597.

Ujino, S., Nishitsuji, H., Hishiki, T., Sugiyama, K., Takaku, H., and Shimotohno, K. (2016). Hepatitis C virus utilizes VLDLR as a novel entry pathway. Proc. Natl. Acad. Sci. U. S. A. *113*, 188–193.

Waldemarsson, J., Areschoug, T., Lindahl, G., and Johnsson, E. (2006). The streptococcal Blr and Slr proteins define a family of surface proteins with leucine-rich repeats: camouflaging by other surface structures. J. Bacteriol. *188*, 378–388.

Weiler, A., Volkenhoff, A., Hertenstein, H., and Schirmeier, S. (2017). Metabolite transport across the mammalian and insect brain diffusion barriers. Neurobiol. Dis. *107*, 15–31.

Materials and methods

Drosophila strains and larval culture conditions

The following fly stocks were used: wolbachia-free w^{1118} (used as reference strain for this work, (Pontier and Schweisguth, 2015)), *mdr65-mtd-tomato (*this study*)*, *mdr65-Gal4* (BDSC 50472, (Pfeiffer et al., 2008; Spéder and Brand, 2014)), *UAS-mCD8-RFP* (BDSC 27399 and 27400*), NP6293-Gal4 ; tub-Gal80*^{ts} (Awasaki et al., 2008)*, UAS-shg-RNAi* (BDSC stock 34831)*, UAS-lpr- RNAi* (VDRC stock 106364)*, UAS-lpr2-RNAi* (VDRC stocks 107597 and 25684)*, UAS-arr-RNAi* (VDRC stock 4818)*, UAS-mgl-RNAi* (VDRC stock 105071)*, yw ; Mi(PT-GFSTF.1)LpR2*$^{MI04745\text{-}GFSTF.1}$(BDSC stock 60219)*, UAS-shi*^{ts} (BDSC stock 44222), *UAS-shi*^{K44A} (BDSC stock 5811)*, yw; EGFP-Rab5* (Fabrowski et al., 2013)*, UAS-GFP-FYVE-myc* (BDSC stock 42716)*, Vkg-GFP* (Buszczak et al., 2007).

Embryos were collected for 2-3 hours on grape juice egg-laying plates. Equivalent numbers (100) of hatching first instar larvae were transferred to standard food plates at 25°C or 29°C (for RNAi knockdown) until mid-third instar larval stage. For the *mdr65-Gal4*, *UAS-RFP x UAS-shi*^{ts}*,* hatching first instar larvae were transferred to standard food plates at 18°C until early-third instar larval stage and transferred then to 30°C.

DNA cloning and Drosophila transgenics

A portion of the *mdr65* enhancer (GMR54C07, Flybase ID FBsf0000165529), which drives in the SPG, was amplified from genomic DNA extracted from *mdr65-GAL4* adult flies, with a minimal Drosophila synthetic core promoter [DSCP(Pfeiffer et al., 2008)] fused in C-terminal. The *mtd-Tomato* DNA codes for a Tomato fluorescent protein tagged at the N-terminal end with Tag:MyrPalm (MGCCFSKT, directing myristoylation and palmitoylation) and at the C-terminal with 3 Tag:HA epitope. It was amplified from genomic DNA extracted from *QUAS-mtd-Tomato* adult flies (BDSC30005, Chris Potter lab). The two amplicons were joined using the Multisite gateway system (Petersen and Stowers, 2011) to generate a *mdr65*^{DSCP}*-mtd-Tomato* construct. The construct was integrated in the fly genome at an attP2 docking site through PhiC31 integrase-mediated transgenesis (BestGene). Several independent transgenic lines were generated and tested, and one was kept (*mdr65-mtd-Tomato*).

Culture of Drosophila brain explants

Staged larvae were washed successively in PBS and ethanol 70% v/v in water then transferred in cold Drosophila Schneider's Medium in a dissection well. Larvae were cut at around a quarter from the posterior spiracle to minimise damages to motor nerves. The posterior part was discarded and the anterior part was turned inside out to expose the brain. All larval tissues were kept except for the gut, which is removed to avoid contamination with intestinal symbiont pathogens. Eight larvae were transferred to one well (24-well cell culture plate: Falcon 353504) and cultured in 750 µl of Culture medium I (Drosophila Schneider's medium (Gibco 217200-24) supplemented with 2 mM L-Glutamine (Gibco 25030-032) and 0.5mM Sodium L-ascorbate (Sigma A4034) at 30°C and 60% humidity under gentle rotary agitation (275 rpm). After 3 h, the Culture medium I is replaced by Culture medium II [Culture medium I supplemented with 1% Fetal Bovine Serum (Sigma F4135)], then the medium was replaced after 3h and every 10h, by a fresh Culture medium II.

Dextran Permeability

We used 10 kDa Dextran (Texas Red, lysine fixable, D-1863, Invitrogen) at 50 mM final concentration in Culture medium II and we followed the same experimental and quantification procedures as described previously (Hatan et al., 2011).

DHE assay

To assess oxidative stress, we performed DHE (dihydroxyethidium) assay following standard procedures (Owusu-Ansah et al., 2008). Briefly, dissected brains were incubated for 5 min in 30 μM DHE, washed three times in PBS and then fixed for 8 minutes in 7% formaldehyde in PBS.

Microorganisms used and culture conditions

The microorganisms that were tested in our experimental set up are shown in Table 1. All strains were grown overnight at 37°C in BHI (Brain Heart Infusion) broth for bacteria or YPD (Yeast extract Peptone Dextrose) medium for fungi. They were stored at -80°C in BHI broth containing 20% glycerol for bacteria or in YPD broth containing 30% glycerol for yeast.

Bacterial glycerol stocks were thawed on Columbia Agar with Sheep Blood plates (Biomérieux 43041) and cultured for 24 h at 37 °C, 5% CO2, 95% humidity. Six single colonies were randomly picked from each plate and used for the inoculation of 8 ml (2 × 4 ml) of Brain Heart Infusion broth (Thermo Fischer Scientific). After 12 h of incubation, 5 ml from each liquid culture were used for the inoculation of 25 ml of Brain Heart Infusion broth. The optical density was measured at 600 nm (OD600), and small adjustments were made by adding fresh broth to bring all OD600 measurements at approximately the same value (around 0.150, time point 0 h). The 30-ml cultures were split into 9 aliquots and 1 aliquot per h was used for OD600 measurement.

Table 1. Microorganisms used in this study

Strains	Relevant characteristics	Reference
Bacteria		
Escherichia coli		
DH5α™-pEGFP-C1	DH5α™ : F– Φ80Δl*acZ*Δ*M15* Δ(*lacZYA-argF*) U169 *recA1 endA1 hsdR17* (rK–, mK+) *phoA* supE44 λ– *thi-1 gyrA96 relA1*	Deghmane et al, 2011
Lactobacillus plantarum		
Lp^{WJL}-GFP		François Leulier
Lp^{WJL}-mCherry		François Leulier
Streptococcus agalactiae		
BM110		Lindahl et al, 2005
COH1		Tettelin et al, 2005
NEM316		Glaser et al 2002
NEM316Δ*cylE*		Forquin et al, 2007
NEM316Δ*srtA*		Lalioui et al, 2005
NEM316Δ*cpsE*		Chaffin et al, 2000
NEM316Δ*lgt*		Henneke et al, 2008
NEM316Δ*lsp*		Henneke et al, 2008
NEM316Δ*lgt/lsp*		Henneke et al, 2008
NEM316Δ*blr*		This study
NEM316Δ*blr* + *blr*		This study
NEM316-GFP		This study
Streptococcus pneumoniae		
ST4		Shaynoor Dramsi
Neisseria meningitidis		
2C4.3-GFP		Muhamed-kheir. Taha
Listeria monocytogenes		
EGDe		Marc Lecuit
Yeast		
Saccharomyces cerevisiae	*MAT a his3Δ1 leu 2Δ0 ura3 Δ0 TPl1-GFP-HI3Mx*	Huh et al, 2003
Candida albicans	CEC4061 *ura3Δ- Δimm434/ura3Δ-Δimm434 his1-hisG/his1arg4Δ-hisG/arg4 RPS1/RPS1-Clp10-PTDH3-GFP*	Christophe D'Enfert
Candida glabrata	*trp1Δ::PTDH3-GFP-AVAL*	Christophe D'Enfert
Cryptococcus neoformans	*H99O-E2-Crimson*	Guilhem Janbon

Construction of NEM316Δ*blr* mutant and complemented strain

In frame deletion mutant of *blr* in NEM316 was constructed by using splicing-by-overlap-extension PCR as previously described (Dramsi et al., 2006). The primers used were the following:

• blr-1Eco 5'-TTCT*gaattc*TGTCGGTGCTGTAATGGAGT-3'

/ blr-2 5'-TAGCTCCGTAAAAGATTAGAGTCCTCCATAAATGT-3'

and

• blr-3 5'-AACATTTATGGAGGACTCTAATCTTTTACGGAGCTA-3'

/ blr-4Bam 5'-TTCT*ggatcc*AACCCCATGATGTAACACT-3'.

The chromosomal gene inactivation was carried out by cloning blr-1/blr-4 fragment into the thermosensitive shuttle plasmid pG+host5. Electroporation of the recombinant plasmid in *S. agalactiae* NEM316 strain and allelic exchange were performed as described (Biswas et al., 1993).

To complement the *blr* mutation in *trans*, the *blr* open reading frame was amplified using:

• pTCVblr-1Bam 5'-TCTC*ggatcc*TTATGGAGGACTCATGAAAG-3'

and

• pTCVblr-9BglII 5'- TCTC*gtcgac*GATTAATGGTGATGATGACC-3' primer

and cloned into the plasmid pTCV downstream from the constitutive promoter Ptet. The resulting plasmid pTCVΩPtet-*blr* was then transformed into competent NEM316Δ*blr* strain.

Construction of GFP expressing NEM316

pMV158GFP is a mobilizable plasmid harboring the *gfp* gene cloned under the control of the P_M promoter (Nieto and Espinosa, 2003). pMV158GFP^{Ery} plasmid was constructed by replacing the Tc resistance gene of pMV158GFP by the *ermB* gene by using the Gibson method (Gibson et al., 2009). Briefly, *ermB* and pMV158-GFP were amplified with Erm-1 5'-GAGGGTGAAATATGAACAAAAA-3' and Erm-2 5'-CCCTTAACGATTTATTTCCTCC-3'primers, and pMV158-3 5'-TTTTATATTTTTGTTCATATTTCACCCTCCAATAATGAGG-3' and pMV158-4 5'-TATTTAACGGGAGGAAATAAATCGTTAAGGGATCAAC-3', respectively. pMV158GFP and PCR product were ligated and the resulting pMV158GFP^{Ery} was used to transform *S. agalactiae* NEM316 strain, applying selection for erythromycin (10 µg/ml).

Bacterial growth curves

One mL of overnight bacterial pre-culture in BHI was washed once in PBS and resuspended at OD600 of 2 mL^{-1}. Then each culture was diluted in a given medium at 1/40 dilution and 180 µl of this suspension dispensed in 96 well plates in triplicate and absorbance measurements were recorded using a Biotek Synergy 2 microplate reader using Gen5 data analysis software (v.3.03).

Drosophila brain explants infection

An overnight preculture was set from glycerol stocks in BHI at 37°C for bacteria or in YPD at 30°C for yeast. The bacterial preculture was diluted 1/20 in BHI, and was grown for 2 h 30 min at 37°C (OD_{600} of 0.8). The yeast preculture was diluted to OD_{600}=0.2 then grown 5 to 6 h at 30°C until OD_{600} of 1. A 10x infectious dose

is then prepared after pelleting through 5 minutes centrifugation at 3,500×g (at 4°C), washing each original culture twice in PBS, twice in Drosophila Schneider's Medium and then resuspended in 750 µl of Schneider's (10 x 10^8 CFU/ml for *Streptococcus agalactiae*, *Streptococcus pneumoniae*, *Listeria innocua* and *Listeria monocytogenes*; 10 x 10^7 CFU/ml for *Neisseria meningitidis*, *Candida albicans* and *Candida glabrata* and 10 x 10^5 CFU/ml for *Cryptococcus neoformans*). Pathogen concentration was calculated by OD_{600} correlation (*Streptococcus agalactiae*, *Streptococcus pneumoniae*, *Listeria innocua* and *Listeria monocytogenes*: 1 OD_{600} = 8,8 x 10^8 CFU/ml; *Neisseria meningitidis*: 1 OD_{600} = 10^9 CFU/ml; *Candida albicans* and *Candida glabrata*: 1 OD_{600} = 3 x 10^7 CFU/ml; *Cryptococcus neoformans*: 1 OD_{600} = 6 x 10^7 CFU/ml).

The10x infectious dose of each pathogen is diluted 1/10 in the brain explant culture medium I to reach the infectious dose (10^8 CFU/ml). Brain explants were infected for 3 h at 30°C and 60% humidity under agitation (275 rpm on a Titramax 100 from Heidolph Instruments). Then, the infected medium was replaced by fresh culture medium II after 3 h and every 10h

***In vivo* Drosophila larval infection**

GBS preculture and culture are prepared as described for the *ex vivo* protocol. 20 nl of concentrated GBS were injected in larvae using the nano-injector Nanoject III (Drummond Scientific) in order to reach 8.8 x 10^8 CFU/ml of hemolymph.

Bacterial quantifications in infected Drosophila brain

The same region of the CNS (Ventral Nerve Cord,VNC) was scanned at an optimised number of slices using a Zeiss LSM880 microscope. The exact number of bacteria for each brain was then determined manually by counting each individual bacterium contained within the boundary of the BBB (*mdr65-mtd-Tomato*).

CFU counts following *in vivo* larval GBS-injection

Each injected larva is washed on a paper with ethanol 70% then bled in 10 µl PBS. The brain is then dissected, transferred and homogenized in 10 µl PBS. The rest of the larval carcass (other tissues except the gut) is also transferred and homogenized in 10 µl PBS. This protocol was done for 5 larvae by condition. Hemolymph, brain and carcass bacterial levels were determined by plating 7 serial tenfold dilutions two times on Columbia Agar with Sheep Blood plates (Biomérieux 43041) and counting of bacterial colonies after 16 hours at 37°C. The average CFU/µl was calculated as an average from all the different dilutions. The bacterial loads per animal were then represented in a Log10 scale, and ratios were calculated from raw counting then represented in a Log10 scale:

• Ratio Brain / Hemolymph = Log10 (cfu per brain / cfu per hemolymph)

• Ratio Brain / Other tissues = Log10 (cfu per brain / cfu per Other tissues)

• Ratio Brain / (Hemolymph+Other tisses) = Log10 (cfu per brain / (cfu per hemolymph+ cfu per Other tissues))

Immunohistochemistry

Brains were processed and stained according to standard procedures. Briefly, brains of inside-out larvae were

fixed for 30 min in 4% methanol-free formaldehyde at room temperature,washed in PBS 3 X 10 min and permeabilised in PBS-Triton 0.3% for 3 × 10 min. Brains were incubated with primary antibodies at 4°C in blocking solution (PBS-Triton 0.3%, Bovine Serum Albumin 5%, Normal Goat Serum 2%) for 18-36 h, then washed with PBS-Triton 0.3% and incubated with secondary antibodies 18-24 h at 4°C in blocking solution, and washed with PBS-Triton 0.3%, Samples were mounted in Mowiol mounting medium and visualised with a laser scanning confocal microscope (Zeiss LSM 880). The following primary antibodies or dyes were used: anti-GBS (homemade), anti-*S.pneumoniae* (homemade), anti-Blr (Waldemarsson et al., 2006), anti-GFP (Abcam), anti-LpR2 (gift from J. Culi), Phalloidin–Atto 647N (Sigma 65906), DAPI (Thermo 62247).

Co-immunoprecipitation and western blot

For each condition, 100 brains of *yw; MiMIC(PT-GFSTF.1)LpR2*$^{MI04745\text{-}GFSTF.1}$ larvae were dissected and lysed in lysis buffer (50mM Tris-HCl [pH 7.5], 150 mM NaCl, 1mM DTT, n-octyl-beta-glucopyranoside 1%, 5mM EDTA, 1mM PMSF, protease inhibitor cocktail Roche). Brain lysates were spun for 10 minutes at 4°C at 15,000×g and incubated 1h at 4°C with 25 µl of equilibrated agarose beads (Chromotek) to prevent non-specific binding to beads. The brain lysates were spun for 2 mins at 4°C at 2,500×g and the cleared supernatant was incubated overnight at 4°C with 25 µl of equilibrated GFP-trap beads (Chromotek). Bound GFP-trap beads were then washed three times, twice with lysis buffer and once with washing buffer.

Bacterial pellets of different GBS strains *WT, Δblr* and *complemented Δblr+blr* were lysed during 1 h at 4°C with 1 ml of lysis buffer. The bacterial lysates were spun for 10 min at 4°C at 15,000×g and the supernatant was incubated for 1 h in 25 µl of equilibrated agarose beads at 4°C. The bacterial lysate was then spun for 2 min at 2,500×g at 4°C and the cleared supernatant was incubated overnight at 4°C in the column containing bound GFP-trap beads. The column was spun for 2min at 2,500×g at 4°C and the beads were washed three times, once with lysis buffer and twice with washing buffer. The beads were then resuspended in Laemmli 4X (BioRad) with 10% of β-mercapthoethanol and heated at 90°C for 10 min.

For western blot, proteins were boiled in Laemmli sample buffer, separated by SDS-PAGE on 7.5% Mini-Protean TGX Stain-Free precast Gels (Bio-Rad, 4568024), and transferred onto PVDF membrane using the Trans-Blot Turbo transfer pack (Bio-Rad). Immuno-detection was performed as follows: the membrane was blocked in PBS–skimmed milk 5% and incubated for 1 hour with rabbit primary anti-Blr (1/750) and mouse primary anti-GFP (Invitrogen, 1/1000) antibodies and then with the secondary Dylight$_{680}$-coupled goat anti-rat antibody (Thermo Scientific Pierce) and HRP-coupled goat anti-rabbit antibody (1/10.000, gift from B. Montagne). Between the two antibodies and before detection, membranes were extensively washed with PBS + 0.1% Tween 20 and detection. was performed combining fluorescence and chemiluminescence (Bio-Rad ChemiDoc). For detection of brain lysate inputs, rat primary anti-GFP (1/1000, Chromotek [3H9]) and HRP-coupled goat anti rat antibody (S. Dramsi).

Serial Electron Microscopy (SEM):

Brains were fixed overnight in 2.5% glutaraldehyde in 0.1 M PHEM buffer pH 7.2. They were washed in 0.1 M PHEM buffer pH 7.2, post-fixed for 1 h and 30 min in 1% osmium tetroxide in 0.1 M PHEM buffer pH 7.2,

and then rinsed with distilled water. Samples were dehydrated through a graded series of 25, 50, 75, 95 and 100% ethanol solutions followed by critical point drying with CO2.
Dried specimens were sputtered with 20 nm gold palladium, with a GATAN Ion Beam Coater and were examined and photographed with a JEOL JSM 6700F field emission scanning electron microscope operating at 7 Kv. Images were acquired with the upper SE detector (SEI).

Transmission Electron Microscopy (TEM):
For transmission electron microscopy, brains were fixed with 2.5% glutaraldehyde in 1X PHEM buffer pH 7.2 overnight at 4°C. Specimens were post-fixed with tannic acid 1% in 0.1M PHEM buffer pH7.2 for 30', post-fixed with 1% osmium tetroxide for 1 hr and 30 min in 0.1M PHEM buffer pH7.2 at room temperature, dehydrated in a graded series of ethanol, and embedded in Epon. After heat polymerization, thin sections were cut with a Leica Ultramicrotome Ultracut UC7' sections (60 nm), stained with uranyl acetate and lead citrate. Images were taken with a Tecnai SPIRIT (FEI-Thermofisher Company at 120 kV accelerating voltage with a camera EAGLE 4K x 4K FEI-Thermofisher Company).

Mouse infection and Ethics statement

All animal experiments in this study were carried out in the Department of Animal Models for Biomedical Research of the Hellenic Pasteur Institute in strict compliance with the European and National Law for Laboratory Animals Use (Directive 2010/63/EU and Presidential Decree 156/2013), with the FELASA recommendations for euthanasia and Guide for the Care and Use of Laboratory Animals of the National Institutes of Health. All animal work was conducted according to protocols approved by the Institutional Animal Care and Use Committee of the Hellenic Pasteur Institute (Animal House Establishment Code: EL 25 BIO 013). License No 6317/27-11-2017 for experimentation was issued by the Greek authorities, i.e., the Veterinary Department of the Athens Prefecture. The preparation of this manuscript was done in compliance with ARRIVE (Animal Research: Reporting of *In Vivo* Experiments) guidelines.

Eight to 10 week-old male CD-1 mice (body weight, 40.99 ± 3.62 g [mean ± standard deviation]) were randomly grouped and injected intravenously (i.v.), via the tail vein, with 10^8 CFU of bacterial suspensions in sterile normal saline. For the determination of bacterial levels in blood and brain, mice were anaesthetized by intraperitoneal (i.p.) injection of a mixture containing ketamine (Imalgene 1000, MERIAL, Lyon, France; 100 mg/kg of body weight) and xylazine (Rompun, Bayer, Leverkusen, Germany; 10 mg/kg of body weight). Blood samples were collected by cardiac puncture. Immediately after, each mouse was euthanized by cervical dislocation and its brain was aseptically removed. One brain hemisphere from each mouse was homogenized in sterile normal saline. Bacterial levels in blood samples and brain homogenates were determined by plating serial tenfold dilutions on Columbia Agar with Sheep Blood plates (Thermo Fischer Scientific, Waltham, MA, USA) and counting of bacterial colonies 16 h later. The numbers of mice in each group of analysis are shown in Table 2. The bacterial loads per animal were then represented in a Log10 scale, and the Brain / Blood ratios were calculated as follows: Ratio Brain/ Blood = Log10 [(cfu / g brain)/(cfu / ml blood)]

Table 2. Sample size per time point per bacterial strain.

	Blood and brain levels				Survival
	3 h	*6 h*	*24 h*	*48 h*	*7 d*
WT NEM316	10	10	18	10	22
Δlgt/Δlsp		12	17	10	10
Δblr	10	10	9		10

Mouse immunohistology

Mice were euthanized by (i.p.) injection of a ketamine/xylazine mix. After transcardial perfusion with 4% paraformaldehyde in phosphate-buffered saline (PBS), the brains of the infected mice were dissected out, post-fixed in the same fixative, cryoprotected in 30% w/v sucrose solution in PBS for 2 d at 4 °C, embedded in O.C.T. compound (VWR Chemicals) and frozen at -80 °C. Series of coronal or sagittal 20 µm-thick sections were collected on Superfrost Plus microscope slides and stored at -20 °C until further processing. The cryosections were thawed and subjected to antigen retrieval in 10 mM sodium citrate solution, pH 6, followed by 1 h blocking of non-specific sites with 5% v/v normal donkey serum (NDS), simultaneously with permeabilization using 0.1% v/v Triton X-100 in PBS. Primary antibodies diluted in 2.5% NDS in PBS were applied overnight at 4 °C, followed by incubation with the appropriate secondary antibodies for 2 h at room temperature. The following primary antibodies were used: rat anti-Cluster of Differentiation 68 (CD68; 1:100; Bio-Rad Antibodies, Oxford, UK; MCA1957GA), rabbit polyclonal anti-ionized calcium-binding adapter molecule 1 (Iba-1; 1:400; FUJIFILM Wako Pure Chemical Corporation, Osaka, Japan; 019-19741), rabbit anti-CD31(1:50; Abcam, Cambridge, UK; ab28364), goat anti-LDLR (1:100, R&D Systems, MN, USA; AF2255), rabbit anti-GBS (1:300; home-made). Secondary antibodies (all from Thermo Fisher Scientific) used for immunofluorescence were conjugated with Alexa Fluor 488 or 546 and cell nuclei were counterstained with 4′,6-diamidino-2-phenylindole (DAPI; 1:1000; Thermo Fisher Scientific). Prolong Gold antifade curing mountant (Cell Signaling Technology, Danvers, MA, USA) was used for mounting. Images were acquired using Leica TCS SP8 confocal microscope.

Image processing

Fiji, Icy or Volocity were used to process confocal data. Adobe Photoshop and Illustrator were used to assemble figures.

Statistical analysis

GraphPad Prism software was used for all analyses.

<u>Drosophila statistical analysis:</u>

- In order to perform statistical tests on several experimental replicates, each value (corresponding to one brain) was normalised to the mean of the control condition within one replicate. Statistical tests were then run on all the normalised values from all replicates, which were considered as biological replicates.
- Comparisons between BBB permeability, GBS entry into the brain, cell viability, oxidative stress, bacterial

levels in the hemolymph, bacterial levels in other tissues, bacterial levels in the brain, ratio of bacterial levels for brain/hemolymph, ratio of bacterial levels for brain/other tissues and ratio of bacterial levels for brain/other tissues+hemolymph were performed by Student's t test (2 conditions) or one-way ANOVA test followed by Tukey's post-hoc analysis (more than 2 conditions) when values followed a normal distribution (assessed by Shapiro-Wilk normality test). Otherwise, non-parametric Mann-Whitney tests (2 conditions) or Kruskal-Wallis tests (more than 2 conditions) were performed.

- Comparison of survival curves was performed using Log-rank test.
- P values lower than 0.05 were considered significant.

Mouse statistical analysis:

- Comparisons between bacterial levels in the blood and the brain, as well as between ratios of bacterial levels for brain/blood were performed by unpaired Student's t test when values followed a normal distribution (assessed by D'Agostino-Pearson normality test). Otherwise, non-parametric Mann-Whitney test was performed.
- Comparison of survival curves was performed using Log-rank test.
- P values lower than 0.05 were considered significant.

Additional references:

Biswas, I., Gruss, A., Ehrlich, S.D., and Maguin, E. (1993). High-efficiency gene inactivation and replacement system for gram-positive bacteria. J. Bacteriol. *175*, 3628–3635.

Buszczak, M., Paterno, S., Lighthouse, D., Bachman, J., Planck, J., Owen, S., Skora, A.D., Nystul, T.G., Ohlstein, B., Allen, A., et al. (2007). The carnegie protein trap library: a versatile tool for Drosophila developmental studies. Genetics *175*, 1505–1531.

Dramsi, S., Caliot, E., Bonne, I., Guadagnini, S., Prevost, M.-C., Kojadinovic, M., Lalioui, L., Poyart, C., and Trieu-Cuot, P. (2006). Assembly and role of pili in group B streptococci. Mol. Microbiol. *60*, 1401–1413.

Gibson, D.G., Young, L., Chuang, R.-Y., Venter, J.C., Hutchison, C.A., and Smith, H.O. (2009). Enzymatic assembly of DNA molecules up to several hundred kilobases. Nat. Methods *6*, 343–345.

Hatan, M., Shinder, V., Israeli, D., Schnorrer, F., and Volk, T. (2011). The Drosophila blood brain barrier is maintained by GPCR-dependent dynamic actin structures. J. Cell Biol. *192*, 307–319.

Morin, X., Daneman, R., Zavortink, M., and Chia, W. (2001). A protein trap strategy to detect GFP-tagged proteins expressed from their endogenous loci in Drosophila. Proc. Natl. Acad. Sci. *98*, 15050–15055.

Nieto, C., and Espinosa, M. (2003). Construction of the mobilizable plasmid pMV158GFP, a derivative of pMV158 that carries the gene encoding the green fluorescent protein. Plasmid *49*, 281–285.

Owusu-Ansah, E., Yavari, A., and Banerjee, U. (2008). A protocol for in vivo detection of reactive oxygen species. Protoc. Exch.

Petersen, L.K., and Stowers, R.S. (2011). A Gateway MultiSite recombination cloning toolkit. PLoS One *6*, e24531.

Pfeiffer, B.D., Jenett, A., Hammonds, A.S., Ngo, T.-T.B., Misra, S., Murphy, C., Scully, A., Carlson, J.W.,

Wan, K.H., Laverty, T.R., et al. (2008). Tools for neuroanatomy and neurogenetics in Drosophila. Proc. Natl. Acad. Sci. U. S. A. *105*, 9715–9720.

Pontier, S.M., and Schweisguth, F. (2015). A Wolbachia-Sensitive Communication between Male and Female Pupae Controls Gamete Compatibility in Drosophila. Curr. Biol. *25*, 2339–2348.

Spéder, P., and Brand, A.H. (2014). Gap Junction Proteins in the Blood-Brain Barrier Control Nutrient-Dependent Reactivation of Drosophila Neural Stem Cells. Dev. Cell 309–321.

Waldemarsson, J., Areschoug, T., Lindahl, G., and Johnsson, E. (2006). The streptococcal Blr and Slr proteins define a family of surface proteins with leucine-rich repeats: camouflaging by other surface structures. J. Bacteriol. *188*, 378–388.

Figure legends

Figure 1: Screening for mammalian neuro-invasive pathogens in a brain explant set-up identifies Group B Streptococcus as able to cross the Drosophila blood-brain barrier.

A. Schematic representation of Drosophila third instar larva showing the brain (grey) suspended in the hemolymph (orange). Top and orthogonal views of the brain covered by the blood-brain barrier (BBB) in brown/dark orange. A'. Schematic representations of the composite Drosophila and mammalian BBBs, which include a layer of extracellular matrix (ECM in grey), a regulatory layer (perineurial glia (PG) and pericytes (PC) in light orange), a barrier layer (subperineurial glia (SPG) and endothelial cells (EC) in dark orange) harbouring strong cell junctions (septate junctions and tight junctions in yellow). Brain cell populations, including neurons are illustrated in blue. A, anterior. P, posterior. D, dorsal. V, ventral.

B. Confocal images of the Drosophila BBB (top view and 3D orthogonal view) labelled for the ECM in grey (*vkg::GFP*), the PG in light orange (*NP6293>GFP*) and the SPG in red (*mdr65-mtd-tomato*).

C. Close-up of septate junctions in green (*Lachesin::GFP*).

D. Sketch of the *ex vivo* protocol to generate infection in Drosophila larval brains. Step 3 depicts confocal images of the brains (top and orthogonal views) stained with phalloidin (white). Pathogens (*L. plantarum* and *S. agalactiae [GBS]*) are stained in green. Orange arrows show GBS inside the brain parenchyma.

E. Close-up of GBS (anti-GBS, green) attached to the SPG (*mdr65-mtd-Tomato*, red) as well as inside the brain. DAPI is in blue.

F. Bacterial count inside the brain 24 h post infection for non-pathogenic *E.coli* (n = 12), *L. plantarum* (n = 14), *GBS BM110* strain (n = 29), *GBS COH1* strain (n = 20), *GBS NEM316* strain (n = 29), and fixed *GBS NEM316* strain (n = 9).

Figure 2: Screening for surface factors identifies the lipoprotein Blr as essential for BBB crossing in Drosophila.

A. BBB permeability tests for non-infected (-) and GBS WT infected brains at 6 h post infection without (black) and with HEPES (purple). ANOVA test: p(- vs GBS WT) < 0.0001; p(- HEPES vs GBS WT HEPES) = 0.0022; p (GBS vs GBS+HEPES) < 0.0001. n(-) = 7, n(GBS WT) = 7, n(- HEPES) = 8 , n(GBS WT+HEPES) = 8.

B. Transmission electron microscopy (TEM) picture of a Drosophila brain infected by GBS WT 6 h post infection, showing the different BBB layers and septate junctions (purple arrow). B'. Close-up of a septate junction.

C. Close-up of a TEM picture of a septate junction in a control brain without infection.

D. Bacterial count inside the brain in GBS entry without (black) and with HEPES (purple) at 6 h (Mann-Whitney test, p = 0.0102). n(GBS) = 17 and n(GBS+HEPES) = 19.

E. Scanning electron microscopy (SEM) picture of GBS WT bacteria attached to the surface of a Drosophila larval brain, under HEPES and at 6 h post-infection.

F. Schematic representation of GBS surface structures and tested virulence factors with corresponding mutants. F'. Schematic structure of Blr lipoprotein.

G-H. Screening of GBS surface structures and virulence factors at (G) 24 h and (H) 6 h post infection identified GBS surface lipoproteins as crucial for BBB crossing. Kruskal-Wallis test. (E) GBS WT (n = 31), GBS-*Δlgt* (p = 0.0124, n=12), GBS-*Δlsp* (p = 0.0022, n = 8), GBS-*Δlgt/lsp* (p < 0.0001, n = 43), GBS-*Δblr* (p < 0.0001, n = 45), GBS-*Δblr*+Blr (p > 0.9999, n = 13), and GBS+Blr (p > 0.9999, n = 15). (F) GBS WT (n = 19), GBS-*Δlgt/lsp* (p < 0.0001, n = 22), GBS-*Δblr* (p = 0.0029, n = 16).

I-J. SEM picture of (I) GBS WT and (J) GBS *Δblr* bacteria attached to the brain surface.

Figure 3: Drosophila lipoprotein receptor LpR2 mediates transcellular passage of the SPG by GBS through endocytosis.

A. A knock-down screen for Drosophila E-cadherin and lipoprotein receptors (*LpR1, LpR2, arrow* and *megalin*) identified LpR2 as crucial for GBS BBB crossing. Kruskal-Wallis test of each knock-down versus control: control (n = 20); E-cad, p > 0.9999 (n = 5); LpR1, p > 0.9999 (n = 11); LpR2, p = 0.0003 (n = 18); arr, p > 0.9999 (n = 5); Mgl, p > 0.9999 (n = 6).

B. Schematic representation of LpR2 structure and confocal image (top and orthogonal views) of LpR2::GFP genomic knock-in line (green) showing colocalisation of LpR2 on SPG membranes (*mdr65-mtd-Tomato*, red).

C. Co-immunoprecipitation experiment between LpR2::GFP immobilised on beads and bacterial lysates of GBS WT, GBS-*Δblr+Blr* and GBS-*Δblr* and detected with an antibody against Blr. Robust Blr-LpR2 interaction was revealed.

D. GBS brain invasion is endocytosis-dependent. Box-and-whisker representation showing that GBS entry at 6 h post infection was significantly decreased by either knocking down LpR2 or blocking endocytosis (dynamin^{ts} and dynamin^{DN}) specifically in the SPG. Mann-Whitney: p(control vs *SPG>LpR2 RNAi*) = 0.0162; p(control vs *SPG>dynamin^{ts}*) < 0.0001; p(control vs *SPG>dynamin^{DN}*) < 0.0001. Control (n = 25); *SPG>LpR2 RNAi* (n = 10); *SPG>dynamin^{ts}* (n = 12) and *SPG>dynamin^{DN}* (n = 7).

E-F. Colocalisation of GBS (white) with markers for early endosome (Rab5-GFP) and lysosome (Lamp1-GFP) in green within the SPG membrane (*mdr65-mtd-Tomato*, red).

Figure 4: GBS uses a panel of strategies to invade the Drosophila larval brain.

A-B. Close-up confocal images of non-infected (A) and GBS-infected (B) brains at 6 h post infection showing the absence of ColIV::GFP (green) staining at the sites of GBS (red) accumulation (arrowheads).

C. GBS brain entry is not affected, 24 h post-infection, after knocking down E-Cadherin and lipoprotein receptors in the PG of Drosophila. ANOVA test: - (n = 14); E-cad, p = 0.9885 (n = 8); LpR1, p = 0.9858 (n = 7); LpR2, p = 0.4932 (n = 6); arr, p = 0.9886 (n = 6); Mgl, p = 0.8845 (n = 7).

D-E. Confocal images of non-infected (D) and GBS-infected (E) brains showing PG membrane (*NP6293>mCD8-GFP*, green) alteration at 6 h post-GBS infection.

Figure 5: An *in vivo* model of brain infection in Drosophila identifies Blr as a virulence factor and confirms LpR2 as a BBB receptor for brain invasion by GBS.

A. Schematic representation of Drosophila third instar larva injected with GBS. Close-up of confocal image showing GBS (in green) inside the brain, 4 h after microinjection.

B. GBS brain entry 4 h post-injection for GBS WT (n = 18), GBS-*Δlgt/lsp* (n = 19), GBS-*Δblr* (n = 23) and GBS-*Δblr+Blr* (n = 20). Kruskal Wallis test: GBS-*Δlgt/lsp* p = 0.0168, GBS-*Δblr* p = 0.0039, GBS-*Δblr+Blr* p = 0.6579.

C. Kaplan-Meier survival curves for larvae injected with mock, GBS WT, GBS-*Δlgt/lsp,* GBS-*Δblr* and GBS-*Δblr+Blr* (n = 60 for each condition) show that GBS-*Δlgt/lsp* and GBS-*Δblr* are less virulent than GBS WT and GBS-*Δblr+Blr.* Log rank test: p(GBS WT vs mock) < 0.0001; p(GBS WT vs GBS-*Δlgt/lsp*) = 0.0002; p(GBS WT vs GBS-*Δblr*) < 0.0001; p(GBS WT vs GBS-*Δblr+Blr*) = 0.2797, and p(mock vs GBS-*Δblr*) = 0.9686.

D. GBS brain entry at 4 h post injection in control (n = 13) and LpR2 knock-down (n = 24) larvae. Mann Whitney test: p < 0.0001.

E. Kaplan-Meier survival curves for control larvae and larvae in which LpR2 has been knocked down in the SPG (*SPG>LpR2 RNAi*), injected with mock or GBS WT (n = 60 for each condition). Log rank test: p(Control + GBS WT vs *SPG>LpR2 RNAi* + GBS WT) = 0.0565; p(*SPG>LpR2 RNAi* vs *SPG>LpR2 RNAi* + GBS WT) = 0.0344.

Figure 6: Blr is a streptococcal virulence factor in mice involved in BBB crossing by GBS.

A-B. GBS counts in the (A) brain [log10(cfu/g)] and (B) blood [log10(cfu/ml)] of mice inoculated with GBS WT at 3 h (n = 10), 6 h (n = 10), 24 h (n = 18), and 48 h (n=10). Mann Whitney test: p(Brain 24 h vs 48 h) = 0.0002 and p(Blood 6 h vs 24 h) < 0.0001.

C. Confocal images showing GBS WT-GFP (green) attached to and in the capillaries (CD31, red) of the brain parenchyma at 4 h post-injection.

D. Confocal images of sagittal brain sections of mice injected with a fluorescent GBS WT-GFP strain demonstrating the presence of GFP-positive bacteria (green) at the choroid plexus (CP) inside the lateral ventricle (LV; outlined; left image) as well as at the walls of the LV and in the brain parenchyma adjacent to the LV (upper right image), at 24 h post infection. In the lower right image, a representative cluster of GFP-positive bacteria (also positive for anti-GBS; red) detected in the brain parenchyma. Typical streptococcal chains found in the clusters are presented in the inset. Nuclei were counterstained with DAPI and visualised in blue.

E. Kaplan-Meier survival curves of mice intravenously injected with GBS WT (n = 22) or GBS-Δ*blr* (n = 10). Log-Rank test p = 0.0055.

F. The ratio of bacterial counts in the brain versus blood [log10([cfu/g brain]/[cfu/ml blood])] in mice inoculated with GBS-*Δblr* was significantly lower than in mice inoculated with GBS WT, at 3 and 6 h post inoculation (n = 10 for each condition). Student's t test, 3 h: p = 0.0351; 6 h: p = 0.0404.

Figure 7: Proposed model for the mechanisms utilised by GBS during BBB crossing.

GBS destroys the ECM layer and crosses the PG layer through a paracellular mechanism and/or cellular damages, likely supported or enhanced by acidosis. The bacteria adhere to the SPG surface via Blr-LpR2 interaction, allowing its internalisation through endocytosis and leading to its transcellular traversal. In the absence of Blr, GBS uses an alternative, albeit less efficient, mechanism for brain invasion, via SPG damages through an unknown process.

Figure 1

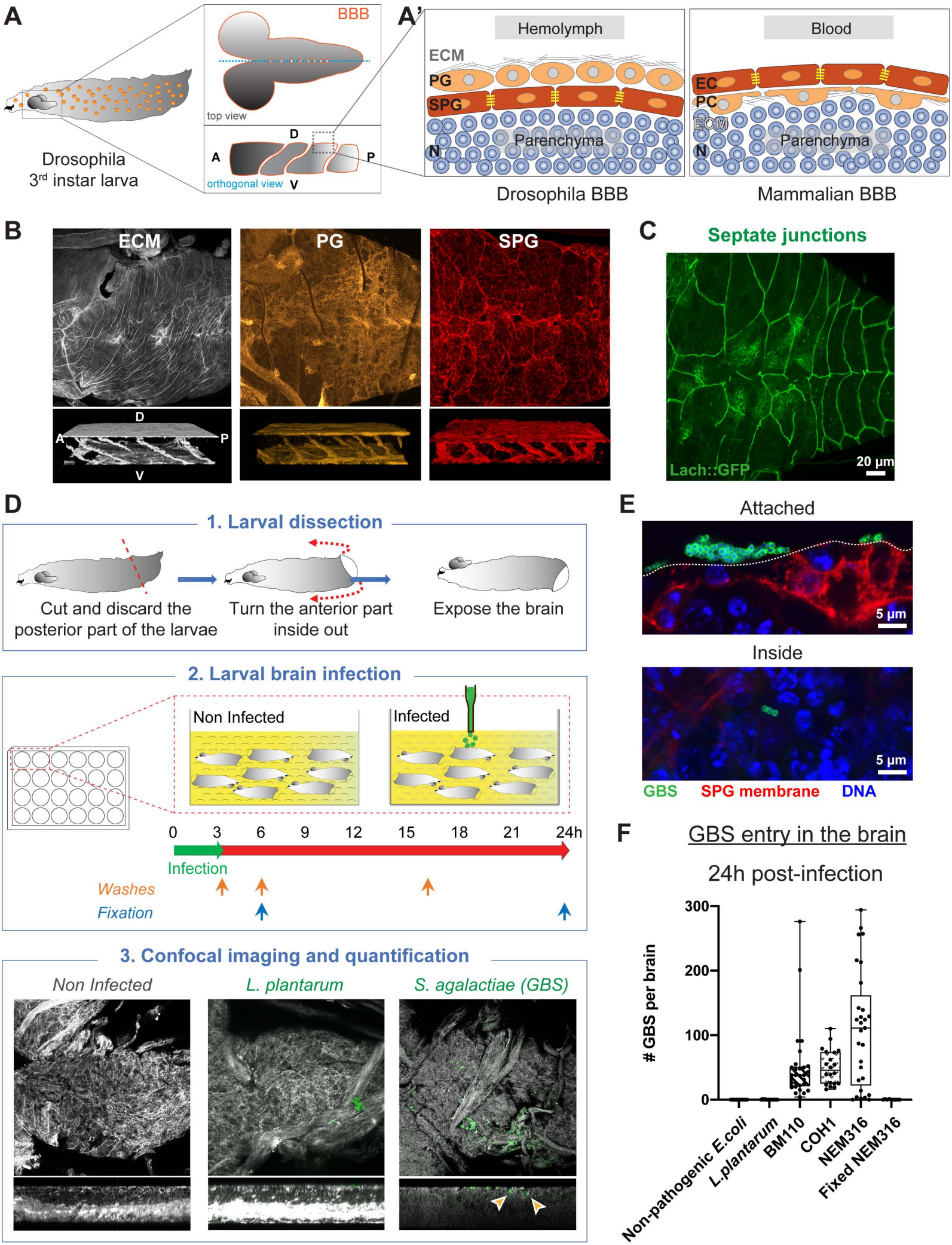
A
BBB
top view
D
A
P
orthogonal view
V
Drosophila
3rd instar larva
A'
Hemolymph
ECM
PG
SPG
Parenchyma
N
Drosophila BBB
Blood
EC
PC
ECM
Parenchyma
N
Mammalian BBB
B
ECM
PG
SPG
D
A
P
V
C
Septate junctions
Lach::GFP
20 µm
D
1. Larval dissection
Cut and discard the posterior part of the larvae
Turn the anterior part inside out
Expose the brain
2. Larval brain infection
Non Infected
Infected
0
3
6
9
12
15
18
21
24h
Infection
Washes
Fixation
3. Confocal imaging and quantification
Non Infected
L. plantarum
S. agalactiae (GBS)
E
Attached
5 µm
Inside
5 µm
GBS
SPG membrane
DNA
F
GBS entry in the brain
24h post-infection
GBS per brain
300
200
100
0
Non-pathogenic E.coli
L.plantarum
BM110
COH1
NEM316
Fixed NEM316

Figure 2

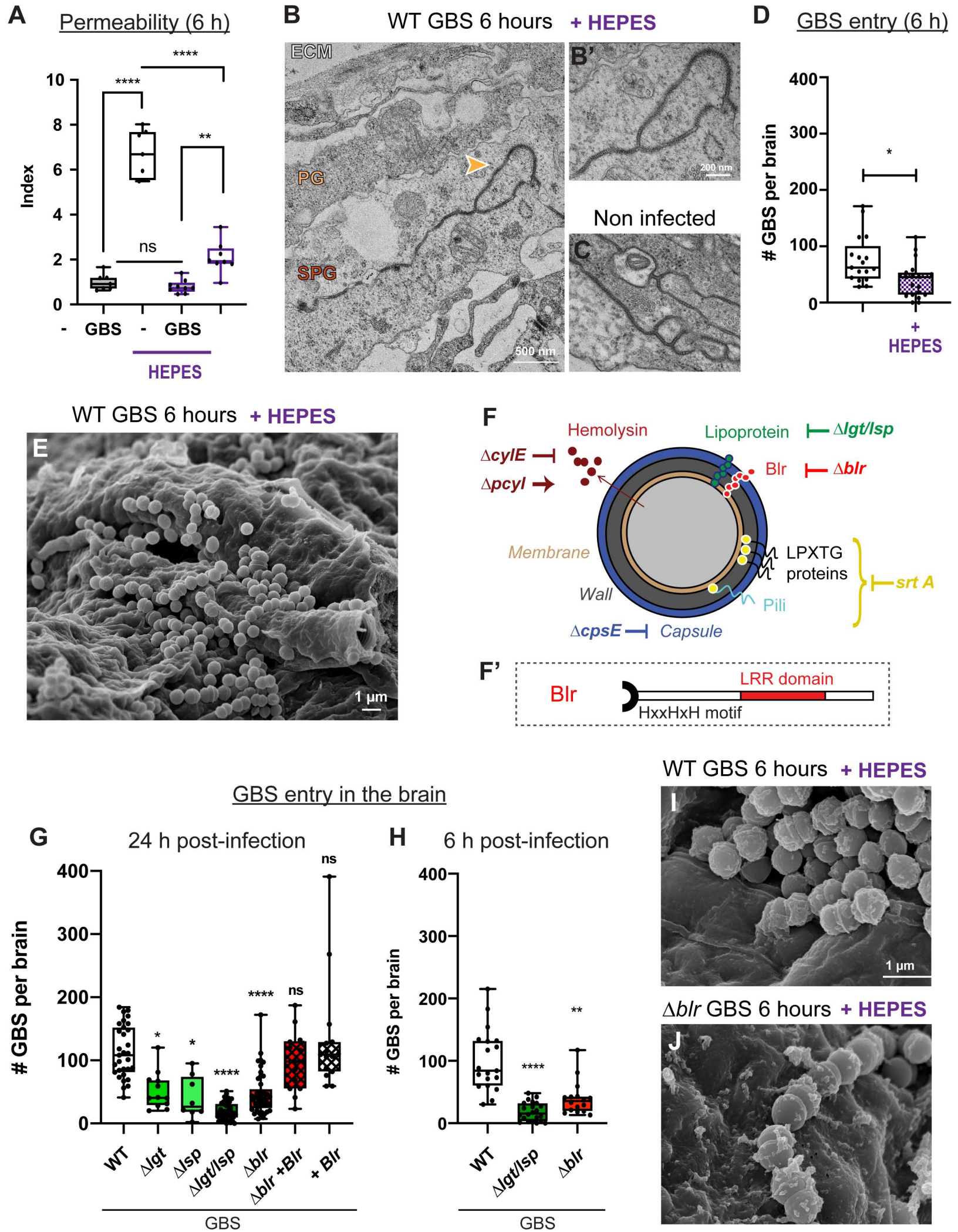
A
Permeability (6 h)
Index
10
8
6
4
2
0
****
****
**
ns
- GBS - GBS
HEPES
B
WT GBS 6 hours + HEPES
ECM
PG
SPG
500 nm
B'
200 nm
Non infected
C
D
GBS entry (6 h)
GBS per brain
400
300
200
100
0
*
+ HEPES
WT GBS 6 hours + HEPES
E
1 µm
F
Hemolysin
Lipoprotein
Δlgt/lsp
ΔcylE
Δpcyl
Blr
Δblr
Membrane
LPXTG proteins
srt A
Wall
Pili
ΔcpsE
Capsule
F'
Blr
LRR domain
HxxHxH motif
GBS entry in the brain
G
24 h post-infection
GBS per brain
400
300
200
100
0
ns
*
*
****
****
ns
WT
Δlgt
Δlsp
Δlgt/lsp
Δblr
Δblr +Blr
+ Blr
GBS
H
6 h post-infection
GBS per brain
400
300
200
100
0
****
**
WT
Δlgt/lsp
Δblr
GBS
WT GBS 6 hours + HEPES
I
1 µm
Δblr GBS 6 hours + HEPES
J

Figure 3

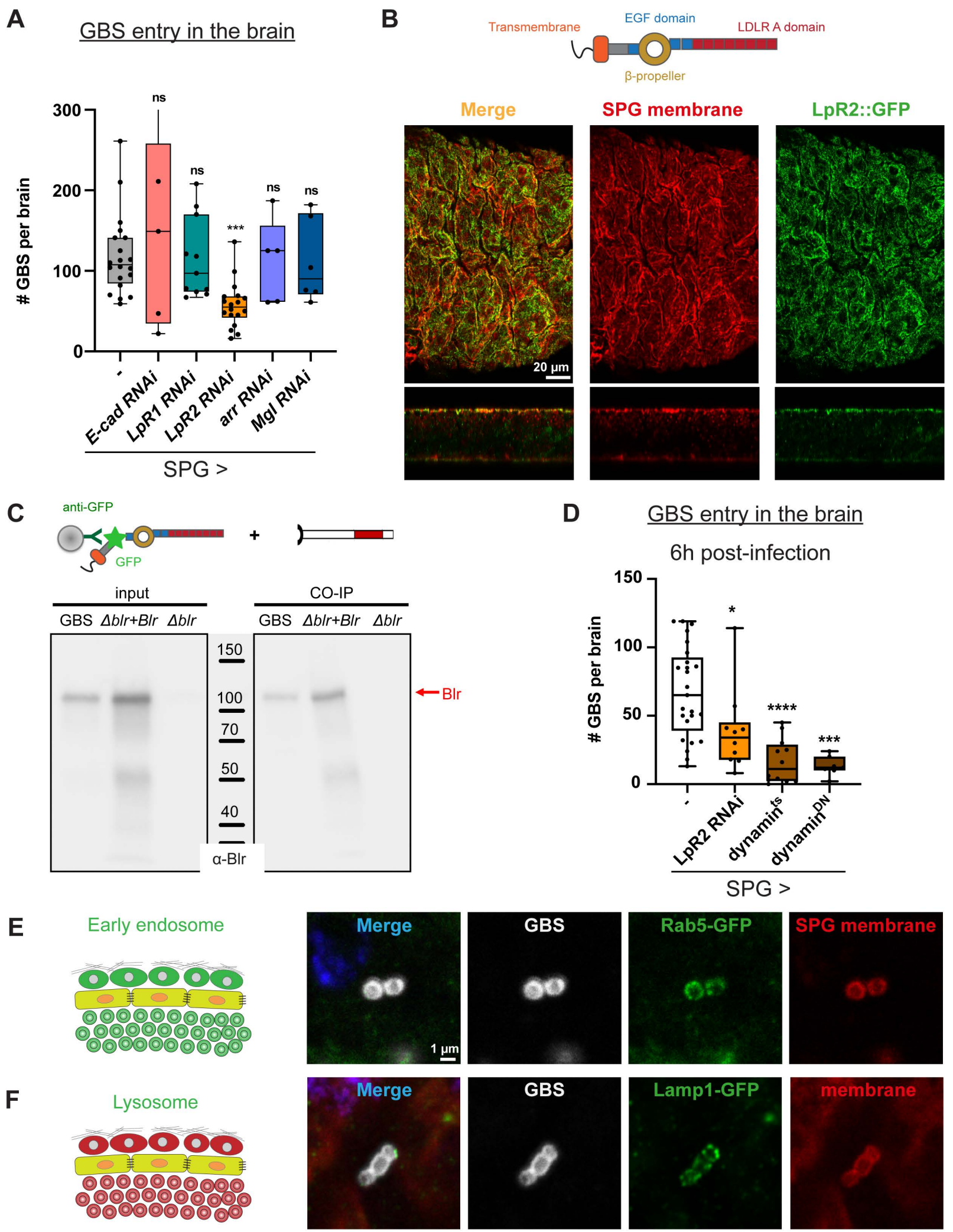
A
GBS entry in the brain
GBS per brain
300
200
100
0
ns
ns
***
ns
ns
-
E-cad RNAi
LpR1 RNAi
LpR2 RNAi
arr RNAi
Mgl RNAi
SPG >
B
Transmembrane
EGF domain
LDLR A domain
β-propeller
Merge
SPG membrane
LpR2::GFP
20 µm
C
anti-GFP
GFP
+
input
CO-IP
GBS
Δblr+Blr
Δblr
GBS
Δblr+Blr
Δblr
150
100
70
50
40
α-Blr
Blr
D
GBS entry in the brain
6h post-infection
GBS per brain
150
100
50
0
*
****
***
-
LpR2 RNAi
dynamin ts
dynamin DN
SPG >
E
Early endosome
Merge
GBS
Rab5-GFP
SPG membrane
1 µm
F
Lysosome
Merge
GBS
Lamp1-GFP
membrane

Figure 4

Non infected

GBS 6h post-infection

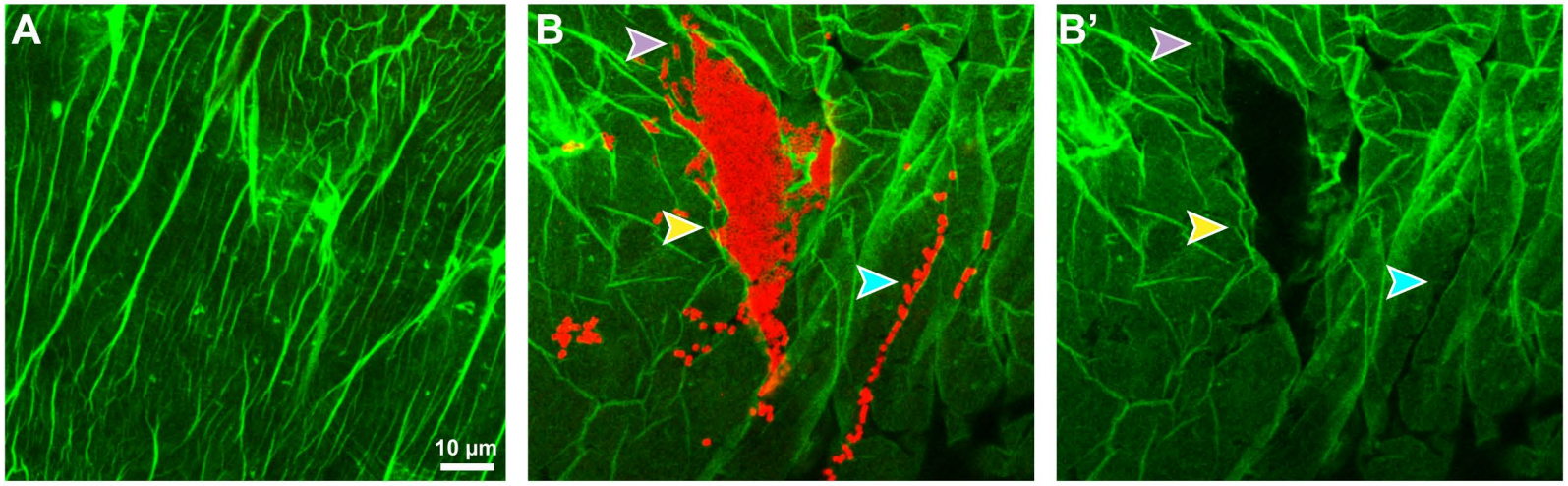

CollV::GFP GBS

C GBS entry in the brain

24h post-infection

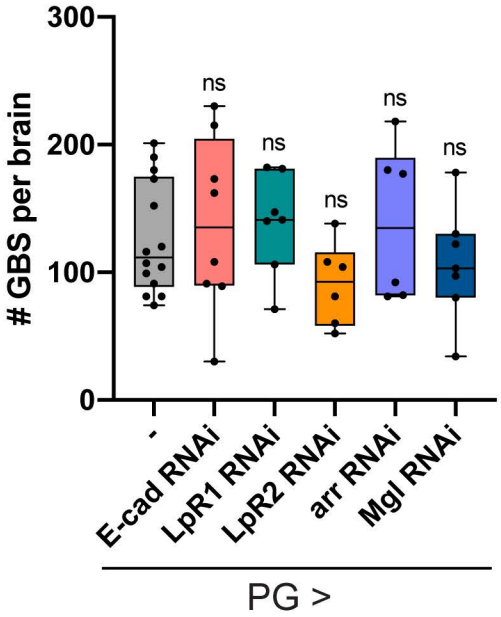

PG > membrane-GFP

Non infected

GBS 6h post-infection

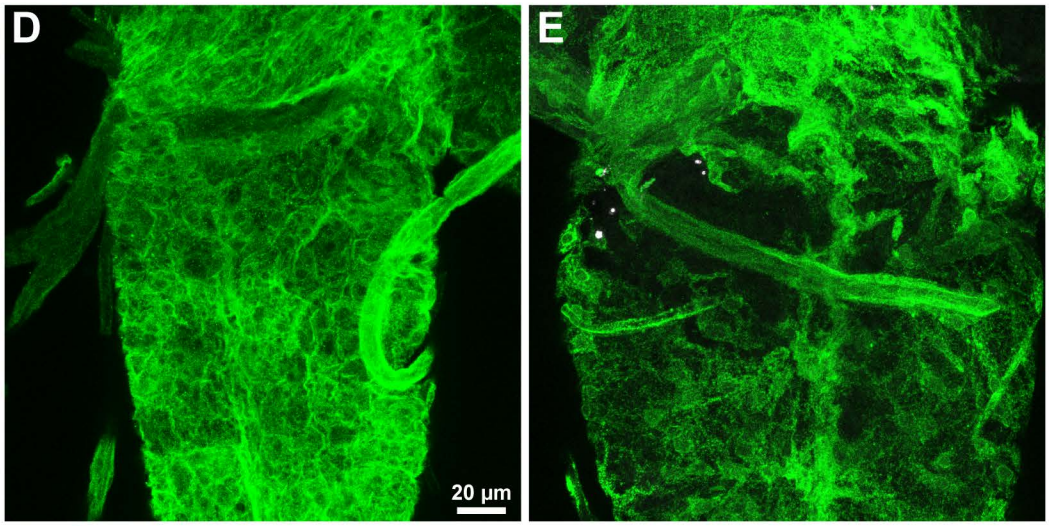

membrane

Figure 5

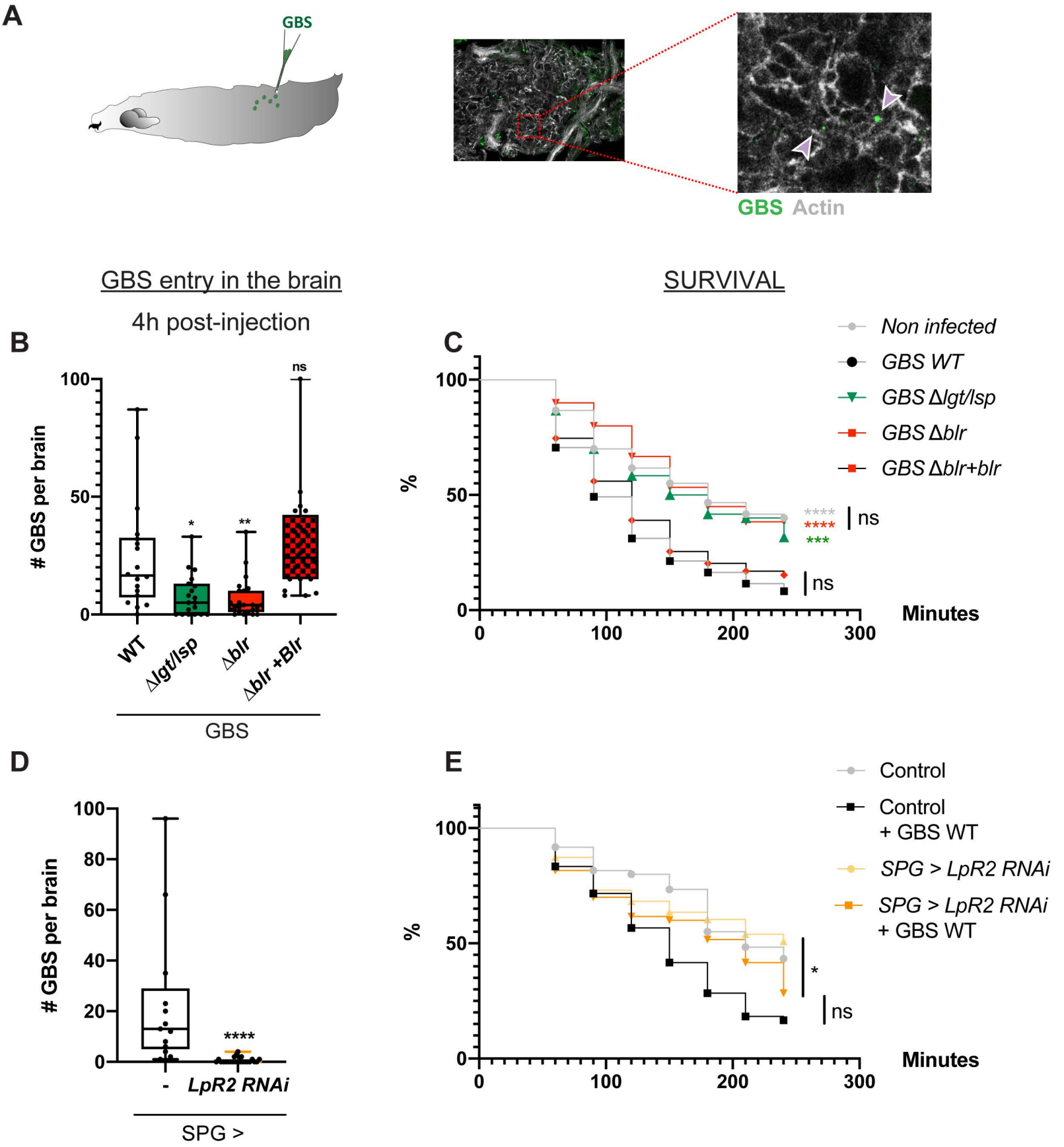
A
GBS
GBS Actin
GBS entry in the brain
4h post-injection
B
GBS per brain
100
50
0
ns
*
**
WT
Δlgt/lsp
Δblr
Δblr +Blr
GBS
SURVIVAL
C
%
Non infected
GBS WT
GBS Δlgt/lsp
GBS Δblr
GBS Δblr+blr
****
****
***
ns
ns
Minutes
0
100
200
300
D
GBS per brain
100
80
60
40
20
0
****
-
LpR2 RNAi
SPG >
E
%
Control
Control
+ GBS WT
SPG > LpR2 RNAi
SPG > LpR2 RNAi
+ GBS WT
*
ns
Minutes

Figure 6

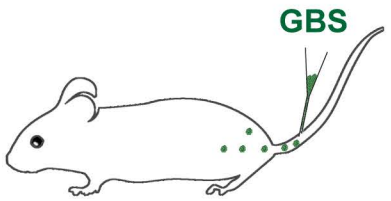

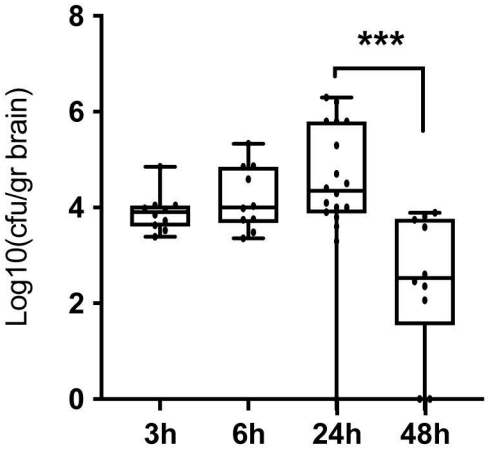

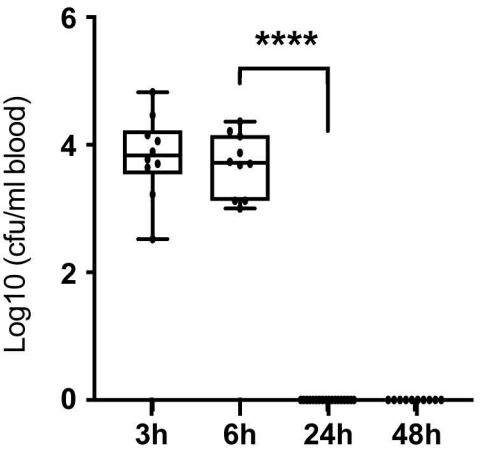

GBS GFP 4h post-infection

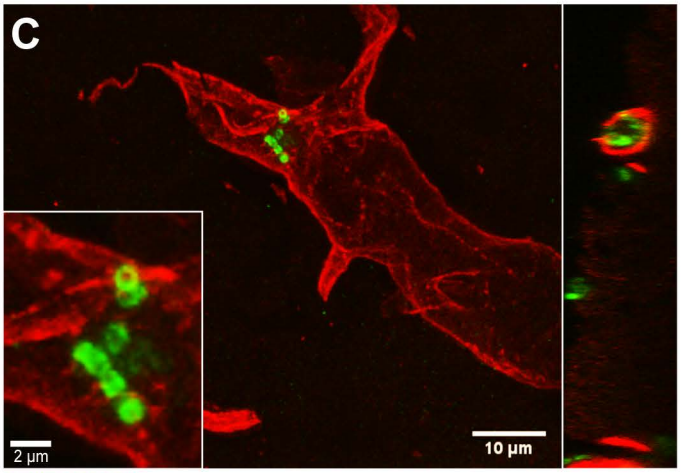

GFP CD31

GBS GFP 24h post-infection

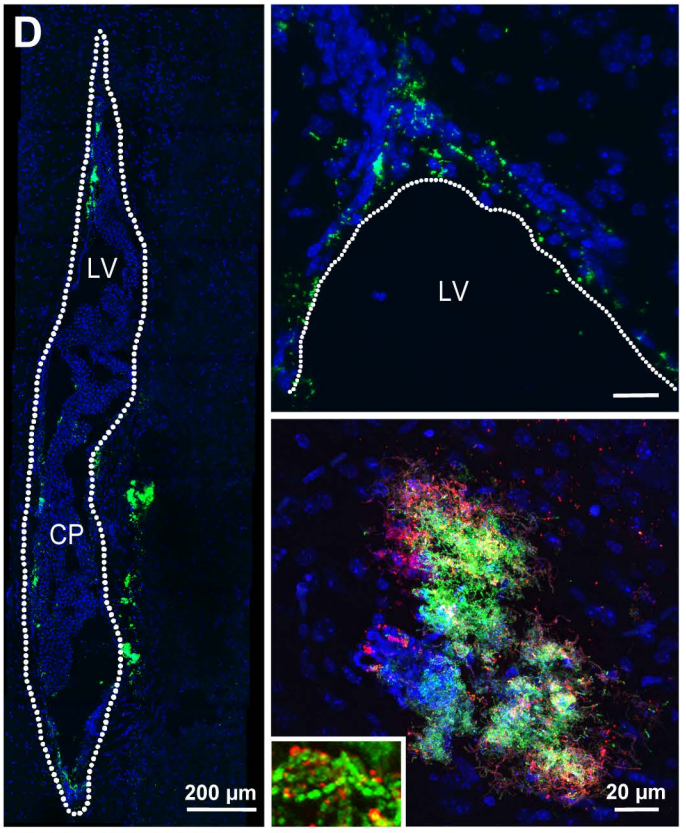

GFP GBS DAPI

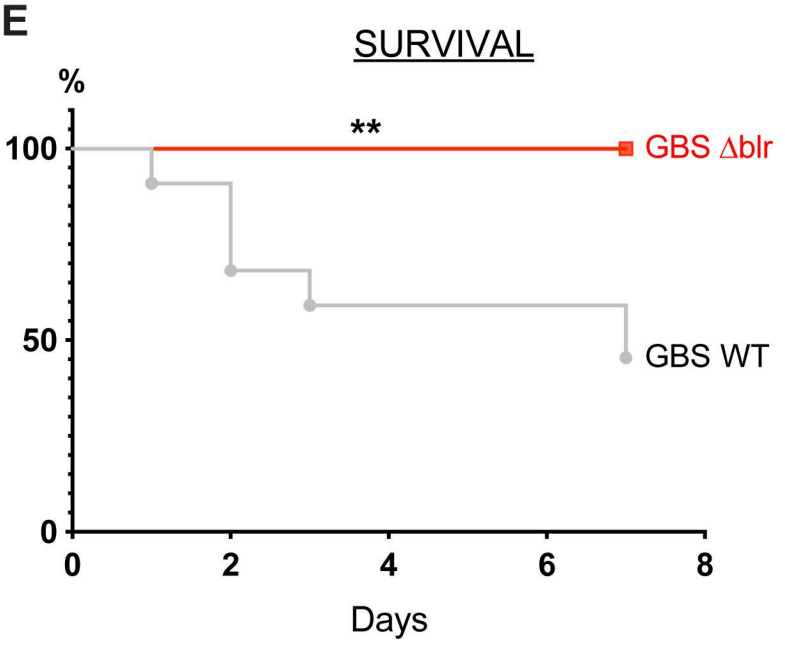

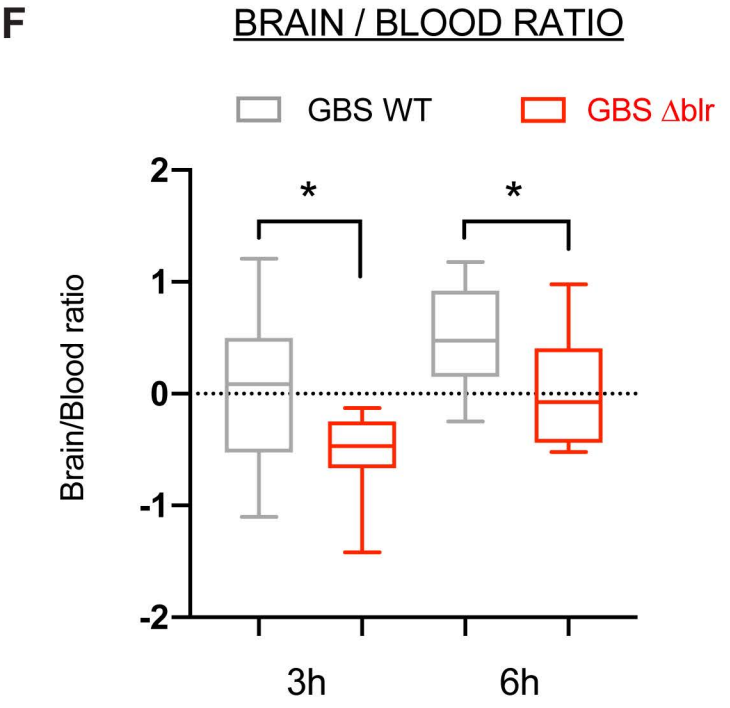

Figure 7

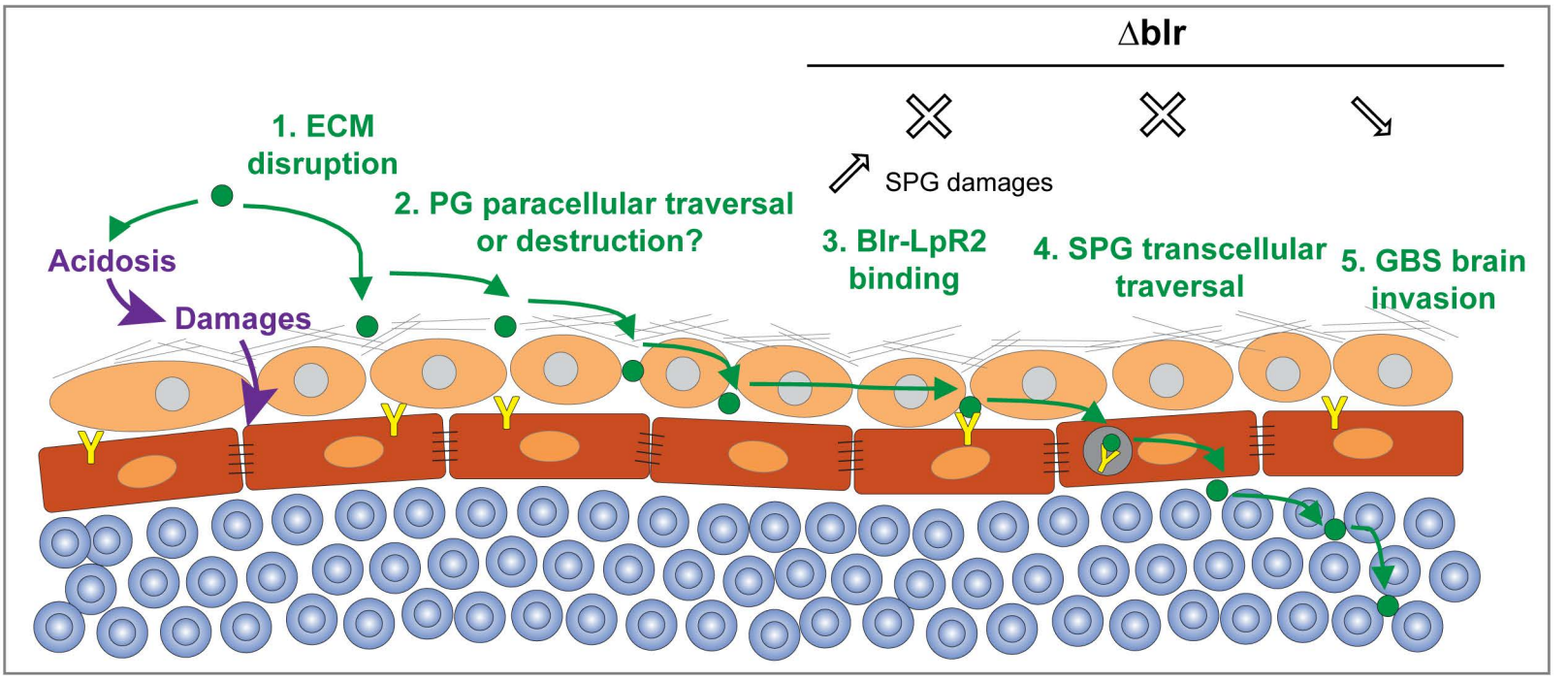
Δblr
SPG damages
1. ECM disruption
2. PG paracellular traversal or destruction?
3. Blr-LpR2 binding
4. SPG transcellular traversal
5. GBS brain invasion
Acidosis
Damages